The symmetrical pattern of base-pair substitutions rates across the chromosome in *Escherichia coli* has multiple causes

Brittany A. Niccum[1], Heewook Lee[2], Wazim MohammedIsmail[3], Haixu Tang[3], and Patricia L. Foster[1]*

[1]Department of Biology, Indiana University, Bloomington, IN, USA, 47405

[2]School of Computer Science, Computational Biology Department, Carnegie-Mellon University

[3]School of Informatics, Computing, and Engineering, Indiana University, Bloomington, IN, USA, 47405

*Corresponding Author:

Patricia L. Foster

Department of Biology

Jordan Hall 447E

1001 East Third Street

Indiana University

Bloomington, IN 47405

812-855-4084

plfoster@indiana.edu

Author email addresses:

Patricia L. Foster, plfoster@indiana.edu

Brittany A. Niccum, brittanyniccum@gmail.com

Heewook Lee, heewookl@cs.cmu.edu

Wazim MohammedIsmail, wazimoha@indiana.edu

Haixu Tang, hatang@indiana.edu

Abstract

Mutation accumulation experiments followed by whole-genome sequencing have revealed that for several bacterial species the rate of base-pair substitutions is not constant across the chromosome but varies in a wave-like pattern symmetrical about the origin of replication. The experiments reported here demonstrate that in *Escherichia coli* several interacting factors determine the wave. Perturbing replication timing, progression, or the structure of the terminus disrupts the pattern. Biases in error-correction by proofreading and mismatch repair are major factors. The activities of the nucleoid binding proteins, HU and Fis, are important, suggesting that mutation rates increase when highly structured DNA is replicated. These factors should apply to most bacterial, and possibly eukaryotic, genomes, and imply that different areas of the genome evolve at different rates.

Keywords *Escherichia coli*, mutation rate, mutation accumulation, whole genome sequencing, mismatch repair, replication timing, nucleoid associated proteins, proofreading

Introduction

Recent studies of mutations accumulated non-selectively across bacterial chromosomes have revealed that rates of base-pair substitutions (BPSs) vary 2- to 4- fold in a wave like pattern that is mirrored in the two independently replicating halves of the chromosome. Such symmetrical patterns have been observed in mismatch-repair (MMR) defective strains of *Escherichia coli* (1), *Vibrio fischeri*, *V. cholerae* (2-4), *Pseudomonas fluorescens* (5), and *P. aeruginosa* (6). Such variation in mutation rates

44 may affect the rate at which genes in different regions of the chromosome evolve, and may exert
45 selective pressure on gene placement. Yet the causes of this variation are not known.
46 The fidelity of DNA replication, which, in *E. coli*, is about 1 mistake in 1000 generations (7), is
47 determined by the intrinsic accuracy of the DNA polymerase and error correction by proofreading and
48 mismatch repair (reviewed in (8, 9). In *E. coli*, proofreading is performed by epsilon, a subunit of the
49 DNA polymerase III holoenzyme. If the polymerase inserts the incorrect base, epsilon's 5' to 3'
50 exonuclease activity degrades a few bases of the new strand and polymerase then re-synthesizes it.
51 The accuracy of DNA synthesis is improved about 4000-fold by proofreading (10). Mismatch repair is
52 performed by three proteins, MutS, MutL, and MutH. MutS recognizes a mismatch and recruits MutL.
53 Together they find a nearby GATC site in which, in *E. coli*, the A is methylated by the Dam methylase.
54 Because methylation lags behind replication, unmethylated As identify the "new", and presumably
55 error-containing, DNA strand. MutH is recruited by MutSL to the GATC site and activated to nick the
56 unmethylated DNA strand, which is then degraded past the mismatch by the concerted activity of the
57 UvrD helicase and one of four exonucleases. Pol III then re-synthesizes the strand. MMR improves the
58 accuracy of DNA replication 100 to 200 fold (11).
59 In our previous study of the BPS density pattern in MMR-defective *E. coli* (1), we correlated
60 mutation rates to the chromosomal sites that are affected by two nucleoid-associated proteins (NAPs),
61 HU and Fis. We suggested that when the replication fork encounters regions of the chromosome with
62 high superhelical density due to the binding of these NAPs, the mutation rate increases. An alternative
63 explanation ties mutation rates to replication timing (2, 3). An intriguing hypothesis is that mutation
64 rates vary in concert with fluctuations in dNTP concentration when the replication origin fires
65 repeatedly during rapid growth (2).

66 In the work presented here, we investigate further the causes of the wave-like pattern of BPS
67 rates. MMR-defective strains of *E. coli* additionally defective for other activities were used in mutation
68 accumulation (MA) experiments and the mutations identified by whole genome sequencing (WGS). We
69 also investigated the effects of different growth conditions on BPS rates. We conclude that the BPS
70 density pattern does not have a single cause, but is the result of several factors affecting DNA
71 replication, repair, and chromosome structure. In addition, we report that a MMR-defective *Bacillus*
72 *subtilis* also has a wave-like BPS density pattern that is symmetrical about the origin of replication.

73 ## Results

74 **The base-pair substitution (BPS) density pattern in mismatch repair-defective strains**

75 In a previous paper (1) we demonstrated that the density of BPS that accumulated across the
76 chromosome in a MMR-defective strain during an MA experiment fell into a wave-like pattern that was
77 symmetrical about the origin. We have since performed nine additional MA experiments with MMR
78 mutant strains, each experiment resulting in the accumulation of over 1000 BPSs, for a total of 30,061
79 BPSs (11). As shown in Figure 1A, the wave-like BPS density pattern was reproducible among the 10
80 experiments. Also as shown in Figure 1A, the mutational density pattern does not exactly match the
81 non-interacting chromosomal macrodomains (MCs) as defined by Valens et al, 2004 (12). In particular,
82 the wave pattern of BPSs is symmetrical about the origin whereas the Ori MC is not.

83 Following the analysis of Dillon et al, 2018 (2), we computed the wavelet coherence of the
84 collected MMR^{-} data taken in the clockwise and the counterclockwise directions around the
85 chromosome; supplementary Figure S1A shows that, except for some asymmetry at the midpoint, the
86 wave is symmetrical across the chromosome. The coherence is greatest between 800 to 1,600 Kb per
87 cycle (= 8 to 16 bins per cycle), which is a similar result to that found by Dillon et al, 2018 (2). We also

88 computed the wavelet coherence of the collected MMR⁻ data against each of the experimental results
89 discussed below, and these graphs are also given in the supplementary figures In the analyses below,
90 the combined data from the 10 experiments with MMR-defective strains are used as the standard to
91 which the results obtained in other genetic backgrounds are compared.

92 The spectrum of BPSs in the MMR-defective strains is dominated by A:T transitions at
93 5'NAC3'/3'NTG5' sites (11). To test if the mutational density pattern was simply due to the distribution
94 of these sites, we removed all the A:T transitions at 5'NAC3'/3'NTG5' sites from the data set. As shown
95 in supplementary Figures S5A, S6A, and Tables 1 and 2, although the mutation rate was reduced by
96 60% when these BPSs were removed, the remaining 12,542 BPSs fell into the same wave pattern. Thus,
97 the variation in BPS rates must be reflective of regions of the chromosome and not the distribution of
98 the hotspot DNA sequences.

99 **Transcription**

100 One obvious hypothesis is that the mutational density pattern reflects transcriptional patterns.
101 Mutation rates have been reported to be both increased (13) and decreased (14) by high levels of
102 transcription. In a previous paper (7) we reported that highly expressed genes had normal mutation
103 rates, a finding that was confirmed in a recent study using deep sequencing to detect mutations (15).
104 To determine if, nonetheless, transcription influences the wave pattern, we used RNA-Seq to
105 quantitate the RNA levels in a Δ*mutL* mutant strain in the lag, exponential, and stationary phases of
106 growth. These results should be representative of the cells in colonies during our MA experiments. We
107 then compared these results to the BPS density pattern by binning the RNA-Seq results into the same
108 bins as used for mutational data. As shown in Figure 1B and supplementary Figure S1B, there was no
109 similarity in the two data sets.

110 Because ribosomal operons are homologous, we could not call SNPs in these genes. The RNA
111 reads from the genes in ribosomal operons were also removed from the RNA-Seq data, but their
112 positions have been indicated in Figure 1B. Interestingly, bin 35, which includes the ribosomal *rrnG*
113 operon, has a high number of RNA reads even in the absence of reads from the *rrnG* genes. This high
114 level of expression is almost exclusively due to the *ssrA* gene, which encodes transfer-messenger RNA
115 (16), that is highly expressed under all three conditions (the RNA-Seq data will be further analyzed in a
116 subsequent paper). The BPS density pattern of several of the strains that will be discussed below tends
117 to reach a minimum in this general area, but it is as often at bin 33 as at bin 35. Given that the bin size
118 is 100 Kb, it seems unlikely that the high level of transcription level of *ssrA*, located in the middle of bin
119 35, is causing these patterns.

120 **Replication Initiation**

121 The BPS density pattern is centered on *oriC*, the origin of replication, and over many experiments
122 in different genetic backgrounds the pattern around the origin has proved to be stable. In both
123 replichores BPS rates decline to a minimum about 300 Kb from the origin and then increase until a
124 peak is reached about 900 Kb from the origin. Mutation rates then fall again and reach a minimum
125 about 3/5th of the distance along each replichore.

126 We tested whether replication initiation was responsible for the maintenance of this pattern by
127 performing MA experiments with strains with errant replication start sites. The *rnhA* gene encodes
128 RNase H1, which degrades RNA-DNA hybrids; in the absence of RNase H1, persistent R-loops can
129 initiate aberrant DNA replication and disrupt normal fork migration (17, 18). But an MA experiment
130 with a Δ*rnhA* Δ*mutL* mutant strain showed no difference in the BPS density pattern from that of the
131 Δ*mutL* mutant strain (Figure 1C, Supplementary Figure S1C, Tables 1 and 2), indicating that aberrant

132 replication Initiation does not influence where mutations occur, at least not when a powerful *oriC* is
133 present.

134 To further test the influence of replication initiation on the mutational density pattern, we
135 performed MA experiments with strains that have a 5.1 Kb region containing *oriC* moved to the
136 midpoint of the right replichore, where it is called *oriZ* (19). These strains are derived from *E. coli* K12
137 strain AB1157, instead of MG1655 strain, the ancestor of our MA strains, and have a large inversion in
138 the right replichore that relieves the head-on collision between replication initiating at *oriZ* and
139 transcription of the *rrnCABE* operon (20). As a control we created an AB1157 Δ*mutL* mutant strain,
140 which had the similar wave-like BPS density pattern as our MMR⁻ strains, indicating that the pattern is
141 intrinsic to *E. coli* K12, not specific to sub-strain MG1655 (Supplementary Figures S5B, S6B, Tables 1
142 and 2). We performed MA experiments on Δ*mutL* derivatives of two additional strains: one with both
143 *oriZ* and *oriC* (WX320 Δ*mutL*), and one with only *oriZ* (WX340 Δ*mutL*). The strain that contained two
144 origins had a similar BPS density pattern as the MMR⁻ strains (Figure 1D, Supplementary Figure S1D,
145 Tables 1 and 2), suggesting that, under our conditions, firing of *oriZ* could not overcome the influence
146 of *oriC*. However, the strain containing only *oriZ* showed a decrease in BPS rate in the 200Kb-area
147 surrounding the new origin, similar to that normally observed about *oriC* (Figure 1E, Supplementary
148 Figure S1E, Tables 1 and 2).

149 **SeqA**

150 As mentioned above, in *E. coli* the adenines in GATC sites are methylated by the Dam
151 methylase. The SeqA protein binds to hemimethylated GATC sites, many of which are clustered around
152 OriC, and, by so doing, SeqA occludes the replication initiation protein, DnaA, hindering origin firing.
153 Sequestering of the origin persists for about one third of a generation; however, the mechanism of

154 relief is not clear. In the absence of SeqA, unregulated initiation presumably results in over-replication,
155 at least when cells are rapidly growing in rich medium (21). Downstream events, such as replication
156 fork collapse, add to the phenotypes of *seqA* mutant cells (22).

157 Loss of SeqA affects chromosomal structure in areas distant from OriC. By binding to
158 hemimethylated DNA, SeqA forms complexes behind the replication fork as it progresses around the
159 chromosome (21). In addition, SeqA binds to areas of the chromosome with closely spaced GATC sites,
160 as well as to particular genes regulated by GATC methylation (23). In the absence of SeqA the
161 superhelicity of the chromosome increases, the nucleoid condenses (24), and transcription is altered
162 (25).

163 To test whether SeqA affects the BPS density pattern, we performed an MA experiment with a
164 Δ*mutL* Δ*seqA* mutant strain. As shown in Figure 1F, Supplementary Figure S1F, and Tables 1 and 2, loss
165 of SeqA somewhat amplified the BPS density pattern of the right replichore, but the pattern was still
166 highly correlated to that of right replichore of the MMR-defective strains. However, the pattern in the
167 left replichore was disrupted in the Δ*seqA* Δ*mutL* mutant strain. Based on chromatin
168 immunoprecipitation analysis, this area of the left replichore is not targeted by SeqA to a greater
169 extent than the same area of the right replichore (23, 26), suggesting that the disruption of the
170 mutational pattern is not due to loss of binding by SeqA. As shown in Figure 1B, bins 44, 38, 37, and 35
171 contain a number of highly expressed genes; in addition, bins 42 and 35 contain highly transcribed
172 ribosomal RNA genes. Thus, we hypothesize that loss of SeqA makes the replication machinery
173 particularly susceptible to interference by transcription, disrupting the mutational pattern. If this
174 hypothesis is correct, the interference apparently makes replication more accurate, perhaps by slowing
175 the speed of DNA polymerase.

176 **Replication Fork Progression**

177 In a recent report, Dillon *et al*., 2018 (2), hypothesized that the periodic variation in mutation
178 rates across the chromosome was tied to the timing of DNA replication. Cellular levels of dNTPs are
179 controlled by ribonucleotide reductase (RNR), the expression of which increases when the origin fires
180 (27, 28) }. In fast-growing bacteria in which new rounds of replication are initiated before cell division,
181 the levels of dNTPs should be high when each origin fires, but then fall as progression of the multiple
182 forks dilute the dNTPs. High levels of dNTPs are predicted to increase the probability of
183 misincorporation, and thus the mutation rate, whereas low levels of dNTPs should slow replication and
184 improve fidelity. This systematic fluctuation in dNTP levels could account for the pattern of mutational
185 density across the chromosome (2).

186 This hypothesis can be tested by examining the wave pattern from several experiments that we
187 have already published (11). The number of replicating chromosomes is a positive function of the cell's
188 growth rate (29). When Δ*mutL* or Δ*mutS* mutant strains were grown on glucose minimal medium,
189 which reduces the growth rate about 2-fold relative to growth on LB, the BPS density pattern became
190 chaotic (Figure 2A, Supplementary Figures S2A, S5C, S6C, Tables 1 and 2). Supplementing the minimal
191 medium with just enough LB to increase the growth rate to normal restored the wave-like BPS density
192 pattern (Figure 2B, Supplementary Figure S2B, Tables 1 and 2). Growing the cells on diluted LB, on
193 which the growth rate was the same as on minimal glucose medium, also preserved the wave-like BPS
194 density pattern (Figure 2C, Supplementary Figure S2C, Tables 1 and 2). When the cells were grown at a
195 lower temperature, which also reduced the growth rate 2-fold, the overall shape of the BPS density
196 pattern was retained, but the increases in BPS rates that normally peak at about 900 Kb from each side
197 of the origin were shifted about 200 Kb further from OriC (Figure 2D, Supplementary Figure S2D, Tables

198 1 and 2). In addition, the magnitude of the fluctuation of the BPS rate across the chromosome was
199 doubled. Thus, it appears that growth rate *per se* is not a major determinant of the BPS density
200 pattern, but other factors, such as the composition of the growth medium, are also important. For
201 example, the expressions and DNA binding characteristics of nucleoid associated proteins (NAPs) are
202 different under different growth conditions (30-32)

203 In *E. coli* growing aerobically dNTP levels are regulated by a Class Ia RNR encoded by the *nrdA*
204 and *nrdB* genes. Although most of this regulation appears to be due to DnaA interactions (28), the
205 NrdR repressor, which regulates a poorly expressed Class Ib RNR, also regulates *nrdAB* transcription;
206 loss of NrdR results in increased expression of RNR throughout the cell cycle (33). Increased RNR
207 should result in increased dNTP levels, and, indeed, the Δ*nrdR* Δ*mutL* mutant strain had twice the
208 mutation rate as the MMR^{-} strains, as expected when dNTP levels are high (Supplementary Table S1).
209 As shown in Figure 2E, Supplementary Figure S2E, Tables 1 and 2, loss of NrdR did not change the basic
210 BPS density pattern, but the peak rate was shifted away from the origin about 200 Kb on each side.
211 This pattern was similar to that observed when cells were grown at low temperature, as described
212 above.

213 Replication fork progression is aided by the accessory replication helicase, Rep, and, in its
214 absence, the time required for chromosome duplication is doubled (34). Rep removes proteins bound
215 to the DNA in front of the fork (34, 35). While these nucleoproteins are primarily transcription
216 complexes (36, 37), Rep could also free the DNA of blocking NAPs. In addition, Rep aids in restarting
217 replication forks after they stall or collapse (38, 39). As shown in Figure 2F, Supplementary Figure S2F,
218 Tables 1 and 2, with the exception of a region close to the origin, loss of Rep disrupted the BPS density

219 pattern across the chromosome, suggesting that slowing or stalling the fork results in a distribution of
220 BPS that is essentially random.

221 **Replication Termination**

222 The results from almost all the strains tested show an increase in the BPS rate in the region
223 where replication terminates. The pattern of this increase varies somewhat among experiments.
224 Usually there are two unequal peaks, as shown in Figure1A, but in some experiments these peaks are
225 better defined and of equal heights and occasionally there is just one peak. We do not know the source
226 of this variation, but suspect it is simply random noise.

227 Replication terminates approximately 180° from the origin in a 1200 Kb region bounded by
228 replication pause (Ter) sites; this region extends from bin 18 to bin 31 in our figures. The anti-helicase
229 Tus protein binds to the Ter sites and allows each replication fork to enter but not to exit, creating a
230 replication fork "trap", within which the two forks fuse and the chromosome dimer is resolved (40). To
231 determine if the interaction of replication forks with Tus contributes to the increased mutation rate
232 within this region, we performed an MA experiment on a Δ*tus* Δ*mutL* mutant strain. As shown in Figure
233 2G, Supplementary Figure S2G, Tables 1 and 2, loss of Tus did not affect the BPS density pattern.

234 The Ter macrodomain (MD) extends from 1200 Kb to 2200 Kb (12), which is roughly from bin 20
235 to bin 28 in our figures. The structure of the Ter MD is maintained by the MatP protein, which binds to
236 23 *matS* sites within this region (41). In the absence of MatP, the Ter MD is disorganized, the DNA is
237 less compact, and the Ter MD segregates too early in the cell cycle and fails to localize properly at
238 midcell (41, 42). Because the mobility of the Ter MD is increased in the absence of MatP, DNA
239 interactions across MD barriers can occur in Δ*matP* mutant cells (41).

240 As shown in Figure 2H, Supplementary Figure S2H, Tables 1 and 2, loss of MatP caused a severe
241 disruption of the BPS density pattern. The mutation rates in the Ter MD were depressed whereas new
242 peaks appeared on either side of the Ter MD in the Right and Left MDs. Interestingly, the BPS pattern
243 near the origin was maintained in the right but not in the left replichore.

244 **Recombination and the SOS response**

245 Homologous recombination is intimately connected to replication. As replication proceeds,
246 various blocks, such as DNA lesions, transcription complexes, and DNA secondary structures, can cause
247 the replisome to pause and to eventually disassemble. This potentially lethal event is prevented by
248 recombination, which can repair and restart the replisome (43). In addition, the termination region is
249 subject to hyperrecombination (44, 45) particularly in the region bounded by TerA and TerB (our bins
250 21 to 24), named the terminal recombination zone (TRZ) (46, 47).

251 Elimination of *E. coli*'s major recombinase, RecA, had a modest effect on the mutational density
252 pattern. As shown in Figure 3A, Supplementary Figures S3A, S5D, S6D, Tables 1 and 2, in the *recA mutL*
253 and *recA mutS* mutant strains, BPS rates declined in bins 21 to 25, corresponding fairly well to the TRZ
254 described above. However, the hyperrecombination within the TRZ is dependent on the recombination
255 pathway defined by participation of the RecBCD complex. When we eliminated RecB, the mutational
256 density pattern did not phenocopy that seen when RecA was absent (Supplementary Figures S5E, S6E,
257 Tables 1 and 2). Either our protocol is not sensitive enough to detect an effect of loss of RecB, or
258 another recombination pathway, *e.g.* RecFOR (48), is sufficient to maintain the mutation rate in the
259 region.

260 In addition to its role in recombination, RecA is also a master regulator of the SOS response to
261 DNA damage, which includes the induction of two error-prone DNA polymerases, DNA Pol IV and V. To

262 test whether these polymerases are involved in determining the BPS density pattern, we performed an
263 MA experiment on a strain deleted for the genes that encode Pol IV, *dinB*, and PolV, *umuDC*. As shown
264 in Figure 3B,Supplementary Figure S3B, Tables 1 and 2, the BPS density pattern in the *mutL dinB*
265 *umuDC* mutant strain was not significantly different than the MMR⁻ pattern. The genes of the SOS
266 response are repressed by the LexA protein; the *lexA3* allele encodes a super-repressor LexA protein
267 that prevents the SOS genes from being induced (49). When this allele was present the BPS density
268 pattern was also unaffected (Figure 3C, Supplementary Figure S3C, Tables 1 and 2). Thus, the SOS
269 response appears to play no role in determining the pattern of BPSs across the chromosome.

270 **Nucleoid Associated Proteins**

271 In a previous report (1), we found that the BPS density pattern of a Δ*mutL* strain was correlated
272 with the density of genes activated by the HU protein and repressed by the Fis protein. Combining
273 these two factors in a linear correlation model accounted for 33% of the variation in the mutational
274 data. HU constrains supercoils and compacts the DNA into nucleosome-like particles; Fis also
275 constrains supercoils but, in addition, bends the DNA (31). While both of these NAPs affect
276 transcription, the general lack of correlation of the BPS rate with transcriptional levels (7); also see
277 above) led us to hypothesize that mutation rates across the chromosome were correlated not with
278 transcription *per se*, but with areas of high DNA structure (1). To further test this hypothesis we
279 preformed MA experiments with MMR⁻ mutant strains also defective for each of a number of NAPs.

280 HU exists as a dimer of its two subunits, HUα and HUβ, encoded by the paralogous genes *hupA*
281 and *hupB*, respectively, in the three possible configurations. While loss of both subunits confers a
282 severe growth defect, loss of only one has little consequence during a normal growth cycle, suggesting
283 they can substitute for each other. HUαβ is the dominant form over most of the cell cycle, but

284 significant amounts of HUα_2 are found during lag phase and early exponential phase, and HUβ_2 is
285 prominent in stationary phase (30). Chromatin immunoprecipitation sequencing (ChIP-Seq) results
286 revealed that HU binds non-specifically to the chromosome and the DNA binding patterns of the three
287 dimers appear to be identical (50).

288 We performed MA experiments with both Δ*hupA* Δ*mutL* and Δ*hupB* Δ*mutL* mutant strains. As
289 shown in Figures 3D, 3E, Supplementary Figures S3D, S3E, Tables 1 and 2, although loss of *hupB*
290 appeared to affect the BPS density pattern, the differences from the MMR$^-$ pattern were not
291 significant. However, loss of *hupA* depressed mutation rates across the chromosome, particularly in the
292 terminus region, while creating new peaks on either side of the Ter MD.

293 Fis has many binding sites across the chromosome, but, based on data at RegulonDB, SOBETZKO *et*
294 *al.* (2012) (51) reported more Fis binding sites in the origin region. However both Chromatin
295 immunoprecipitation plus microarray analysis (ChIP-chip) and ChIP-Seq studies found the density of Fis
296 binding to be more-or-less constant across the chromosome (32, 52). Loss of Fis in both Δ*fis* Δ*mutL* and
297 Δ*fis* Δ*mutS* mutant strains tended to flatten the BPS density pattern across the chromosome except in
298 the region around the origin (Figure 3F, Supplementary Figures S3F, S5F, S6F, Tables 1 and 2).

299 The NAP HNS binds to DNA at its high-affinity binding sites and then spreads by oligomerization
300 along A:T rich regions of DNA. Bridging between HNS-DNA complexes condenses the DNA into a few
301 clusters per chromosome (53-55). However, as shown in Figure 3G, Supplementary Figure S3G, Tables
302 1 and 2), loss of HNS had little effect on the BPS density pattern, and, thus, the long-range structures
303 produced by HNS appear not to affect BPS rates.

304 The DPS protein accumulates in stationary phase cells, condenses the nucleoid into a crystalline-
305 like state, and protects the DNA from oxidative and other damage (56). Despite this radical physical

306 change, loss of DPS had little effect on the BPS density pattern Figure 3H, Supplementary Figure S3H,
307 Tables 1 and 2). Of course, we do not know the degree to which cells in stationary phase contribute to
308 the BPS rates under our experimental conditions.

309 **Proofreading**

310 As mentioned above, epsilon is the proofreading subunit of the DNA polymerase III holoenzyme.
311 The *mutD5* allele encodes an epsilon protein that is inactive for proofreading, and strains carrying this
312 allele have a mutation rate 4000-fold greater than that of wild-type strains, and 35-fold greater than
313 that of MMR-defective strains (10). As shown in Figure 4A, Supplementary Figure S4A, Tables 1 and 2,
314 when proofreading was inactive but MMR was active, the BPS density pattern was less dramatic than
315 when MMR was inactive and proofreading was active; but, nonetheless, the wave pattern was basically
316 the same. When both MMR and proofreading were inactive, which reveals the mutations solely due to
317 replication errors, the BPS density pattern was nearly flat but around the origin it retained significant
318 correlations to the patterns of both the MMR-defective and *mutD5* mutant strains (Figure 4B,
319 Supplementary Figure S4B, Tables 1 and 2). Thus, the pattern of BPS on both sides of the origin appears
320 to be established by replication errors and then elsewhere across the chromosome the density pattern
321 is largely due to differential error-correction by both proofreading and MMR.

322 **Wild-type**

323 The mutational density wave patterns evident in our data, and in data from other bacteria (2, 3),
324 were obtained when MMR was inactive. Thus, the question arises: does the pattern appear in wild-
325 type strains? It is difficult to answer this question because mutation rates in wild-type strains are so
326 low (in *E. coli*, 120-fold lower than that of MMR-defective strains (7, 11) that enormous experiments
327 would have to be conducted in order to accumulate enough mutations to approach statistical

328 confidence. In a recent study we compared the mutation rates and spectra of a number of *E. coli*
329 strains defective in various DNA repair activities; of these, the results from seven strains were
330 indistinguishable from those of the wild-type parent (57). By combining the mutations from these
331 strains, we achieved 1933 BPSs (11), enough to expect to see a wave pattern if it existed. As is evident
332 in Figures 4C, 4D, Supplementary Figures S4C, S4D, Tables 1 and 2, these BPSs did not create fall into a
333 recognizable pattern. Indeed, the pattern from the wild-type strains appears to be random; the
334 variance to mean ratio of the binned mutations is 1.4, indicating the values are not disperse, and the
335 MatLab "runstest", a test for runs, returns a P value of 0.58, also indicating that the bin values are
336 random. In the wild-type strain both MMR and proofreading are active, and, while these two activities
337 have similar correction biases (Figure 4A), proofreading is much more powerful, producing the pattern
338 seen in the MMR-defective strains. Although we cannot conclude that the mutational density pattern
339 in the wild-type strain is other than random, it does have similarity to both the patterns seen in the
340 MMR-defective strains and in the *mutD5* mutant strain, particularly around the terminus (Figures 4C,
341 4D, Supplementary Figures S4C, S4D and Tables 1 and 2).

342 ***Bacillus subtilis***

343 In additional to *E. coli* strains, symmetrical mutational density patterns have been demonstrated
344 in MMR- derivatives of *Vibrio fischeri*, *V. cholera* (2-4), *Pseudomonas fluorescens* (5), and *P. aeruginosa*
345 (6). Here we add *Bacillus subtilis* to this list. As shown in Figure 4E, Supplementary Figure S4E, Tables 1
346 and 2, the BPS mutation rates in a *B. subtilis mutS::*Tn*10* mutant strain fell into a wave like pattern that
347 was symmetrical about the origin. Although similar in shape, the pattern was significantly different
348 from that of *E. coli* (Figure 4E, Supplementary Figure S4F, Tables 1 and 2). However, as in *E. coli*, the

349 BPS rate appeared to increase in the terminus region, which in *B. subtilis* is not 180° from the origin
350 and corresponds to bins 20-24 in Figure 4E.

351 ## Discussion

352 In this report we have examined a number of factors that could be responsible for establishment
353 and maintenance of the symmetrical wave-like BPS density pattern across the chromosome. In broad
354 terms these factors were: transcription; DNA replication initiation, progression, and termination;
355 recombination and the SOS response to DNA damage; the binding of nucleoid-associated proteins;
356 and, error-correction by MMR and proofreading. As discussed above, we found that transcription and
357 the SOS response had little effect, and the effect of recombination was modest and confined to the
358 terminal region. We discuss the more significant, factors in greater detail here.

359 **DNA replication initiation, progression, and termination**

360 Providing additional replication origins, either by eliminating RNase H1 or by inserting an ectopic
361 *oriC* (*oriZ*), did not disrupt the wave (Figure 1C and 1D). However, when *oriZ* was the only origin of
362 replication, the region of depressed BPS rate that surrounds *oriC* when it is in the normal position was
363 re-established about the new origin (Figure 1E). Note that only 5.1 Kb of DNA containing *oriC* was
364 relocated (19), whereas the region of reduced mutation rate is about 200 Kb; thus, the mutation rate is
365 not determined just by the DNA sequence surrounding the origin. We hypothesize that the process of
366 replication initiation protects the DNA from damage and/or newly established replication forks have a
367 low error-rate. In addition, the BPS mutation rate was increased for about 1000 Kb (10 bins) on either
368 side the new origin so that it resembled the same region about the normal origin. The size of this area
369 is close to the same size detected as “interacting zones” around *oriZ* (58). However, the mutational
370 density pattern across the rest of the chromosome did not re-establish itself to be symmetrical about

371 *oriZ*, but remained symmetrical about the absent *oriC*. Thus, other factors must be important at distant
372 regions. We can also conclude that the overall structure of the BPS pattern across the chromosome is
373 not determined by active replication initiation *per se*¸ but may have evolved in response to replication
374 initiation.

375 Both *V. fischeri* and *V. cholera* have multiple circular chromosomes of different sizes; by
376 comparing the mutational density patterns of these chromosomes, Dillon et al, 2018 (2) identified the
377 timing of replication as a significant determinant of the mutational density patterns. As mentioned
378 above, they suggested that the pattern could be the result of variations in the levels of dNTPs as origins
379 fire during rapid growth. Our results provide partial support for this hypothesis, but also indicate that
380 growth on rich medium, not growth rate *per se*, is a significant determinant of the mutational density
381 pattern, possibly because of effects on the expression and DNA binding of HU and Fis (see below). Our
382 results with a Δ*nrdR* mutant strain (Figure 2E) also show that dNTP levels are important, but, again,
383 other factors are driving the overall wave pattern. In addition, the results with the Δ*rep* mutant strain
384 (Figure 2F) indicate that radically interrupting the progression of the replication fork disrupts the
385 mutational density pattern.

386 After declining to a local minimum about 3/5th of the distance along each replichore, mutation
387 rates rise in the terminus region (Figure 1A). We originally hypothesized that this increase was due to
388 collisions of the replication complexes with the Tus anti-helicase, most of which would take place in
389 the region between bins 18 and 31 (1). However, elimination of Tus had no effect on the wave pattern
390 (Figure 2G, Supplementary Figure S2G), refuting this hypothesis. But, eliminating MatP, the protein
391 that maintains the structure of the Ter MD, reduced mutation rates in the Ter MD, suggesting that
392 replication of highly structured DNA is error-prone (Figure 2H, Supplementary Figure S2H).

393 Interestingly, in Δ*matP* mutant cells mutation rates increased in the Right and Left MCs, suggesting
394 that in the absence of MatP, these adjacent regions of DNA gained structure. The mechanism by which
395 MatP structures the Ter MC is not clear (59, 60), but it probably involves supercoils which, when
396 unconstrained, could migrate into adjacent areas. However, two studies have found that loss of MatP
397 increases the mobility and long-range interactions of adjacent DNA (41, 61). Resolution of these
398 conflicts will require further experimentation.

399 *Nucleoid-associated proteins*

400 Our previous results predicted that the NAPs HU and Fis should play a role in establishing or
401 maintaining the wave-pattern of BPS, but HNS should not (1). The results presented here confirmed
402 that prediction. In addition, we also found that Dps had no effect on the BPS density pattern. Because
403 the NAPs affect gene expression in various ways, we cannot conclude that DNA binding by the NAPs
404 themselves is responsible for the mutational pattern. And, indeed, we found no significant positive
405 correlations between the BPS pattern and published binding sites of the NAPs, although the location of
406 the binding sites themselves vary widely among published results (e.g. see (32, 50) and the data in
407 RegulonDB (62). Nonetheless, we favor the hypothesis that structuring of the DNA by the NAPs,
408 directly or indirectly, contributes to the BPS pattern.

409 The local effect of HU binding is to bend the DNA, but dimer-dimer interactions produce higher-
410 order HU-DNA complexes that can constrain negative supercoils (63, 64). The analysis of the effect of
411 HU on the mutational density pattern is also complicated by the variation in the cellular concentrations
412 of the three forms with growth cycle (30). Although the two subunits can compensated for each other
413 for viability, the affinities of three forms of HU for various DNA structures (linear, nicked, and gapped)
414 differ (65). Both HUα_2 and HU$\alpha\beta$ can constrain supercoils, but HUβ_2 apparently cannot, at least *in vitro*

415 (30). Since HUβ is not stable (66), the phenotype of a Δ*hupA* mutant strain may simply be that of low
416 cellular HU concentration.

417 While loss of HUβ had little effect on the mutational density pattern (Figure 3D, Supplementary
418 Figure S3D), loss of HUα reduced the overall BPS rate by 33% and also changed the pattern (Figure 3E,
419 A Supplementary Figure S3E). In the Δ*hupA* Δ*mutL* mutant strain, mutation rates were low in the
420 terminus region but elevated in the Right and Left MCs, very similar to the pattern seen in the Δ*matP*
421 Δ*mutL* mutant strain (Figure 2H). The low mutation rate in the Ter MD corresponds well with the
422 density of genes activated in wild-type cells but not in HU-deleted cells (67). HU regulates transcription
423 by modifying the DNA superhelical density, suggesting that, like MatP, HU increases the structure of
424 the DNA in the terminal region, causing DNA replication to become error-prone.

425 The mutational pattern in the Δ*hupA* Δ*mutL* mutant strain is also similar to that of the Δ*recA*
426 Δ*mutL* strain (Figure 3A). An mutation accumulation experiment with a Δ*hupA* Δ*recA* Δ*mutL* mutant
427 strain resulted in a pattern similar to both single mutant strains, and so was not informative (data not
428 shown).

429 Fis is a major transcriptional regulator, either activating or repressing, directly or indirectly,
430 nearly a thousand genes (52). At some promotors Fis acts as a classic transcriptional regulator by
431 interacting with RNA polymerase, but at other promotors Fis affects gene expression by altering the
432 DNA superhelical density (68). The Fis DNA binding sequence is degenerate and the estimated number
433 of binding sites identified by sequence analysis across the genome varies widely among studies. The
434 results of ChIP analyses also vary: the number of DNA regions associated with Fis in different studies
435 ranges from 200 to 1500, which may reflect the effects of different growth conditions (32, 52, 69).

436 The loss of Fis nearly doubled the overall BPS rate, but flattened the wave pattern outside of the
437 origin region (Figure 3F, Supplementary Figures S5F, S6F). As mentioned above, the mutational density
438 pattern MMR⁻ strains is correlated to the density of genes activated in a Δ*fis* mutant strain as reported
439 by Blot *et al*, 2006 (70). This correlation is particularly strong in bins 14 to 33 (ρ = 0.62, P = 0.003),
440 which corresponds to the area flattened in the Δ*fis* Δ*mutL* and Δ*fis* Δ*mutS* mutant strains. However, no
441 correlation exists between our mutational data and genes found to be responsive to Fis in a recent
442 study (32). Clearly more studies are needed to resolve these conflicts.

443 *Error-correction*

444 Assuming that the BPS recovered from the *mutD5* Δ*mutL* mutant strain are due to intrinsic errors
445 made by DNA polymerase, we conclude that the polymerase is accurate close to the origin, then
446 becomes increasingly less accurate as replication proceeds to about 1/3 of the replichore, at which
447 point accuracy increases again (Figure 4B). The mutational pattern in the MMR-defective strains must
448 reflect the biased ability of proofreader to correct these polymerase errors. Thus, proofreading is
449 effective close to the origin, but then declines for about 1/3 of the replichore, increases in the Right
450 and Left MCs, but declines again in the terminus region (Figures 1A, 4B). Mutations in the *mutD5*
451 mutant strain are due to the failure of MMR to correct the polymerase errors that survive in the
452 absence of proofreading. Since the mutational pattern in the *mutD5* mutant strain mimics that of the
453 MMR-defective strains (Figure 4A, Supplementary Figure S4A, Tables 1 and 2), error correction by
454 MMR, although much less powerful, apparently has the same biases as error correction by
455 proofreader.

456 Given the above considerations, we would expect the mutational density pattern in the wild-type
457 parental strain to mimic that of the MMR-defective strains. However, the nearly 2000 BPS accumulated

458 in eight strains with wild-type mutational phenotypes appear randomly distributed across the
459 chromosome (Figures 4C, 4D). One explanation for this discrepancy is that when both proofreading and
460 MMR are active, the mutation rate is reduced to the point that other, weaker DNA repair and
461 mutagenic activities obscure the underlying pattern. Although not significantly correlated, the wild-
462 type BPS pattern is similar to the MMR$^-$ pattern, particularly around the terminus, supporting this
463 hypothesis. Alternatively, although the eight strains that we combined to produce 2000 BPS have the
464 same mutation rates, they may have different wave patterns that tend to negate each other and
465 obscure the underlying wild-type pattern.

466 ## Conclusions

467 By applying mutation accumulation followed by whole-genome sequencing to bacterial strains mutant
468 in various activities we have determined that the most important factors determining the symmetrical
469 pattern of BPS rates across the chromosome are: the initiation, progression, and termination of DNA
470 replication, replication error-correction, and chromosome structure. Because of the conservation of
471 these factors, our results should apply to most bacteria, and possibly eukaryotes, and imply that
472 different regions of the genome evolve at different rates.

473 ## Methods

474 **Bacterial Strains and Media**

475 The strains used in this study are listed in Supplementary Table S1 and the methods of their
476 construction are in Supplementary file: Materials and Methods. Standard media and antibiotics were
477 used (see Supplementary file: Material and Methods).

478 **Mutation accumulation experiments**

479 The complete MA procedure has been extensively described (7, 11, 57). Details are given in the
480 Supplementary file: Material and Methods

481 **Genomic DNA Preparation, Library construction, Sequencing, and Sequence Analysis**

482 Details are given in the Supplementary file: Material and Methods.

483 **RNA sequencing**

484 The *E. coli* strain PFM144, which is PFM2 Δ*mutL* (11), was grown in LB and aliquots collected
485 during lag (OD = 0.022), log (OD = 0.3), and stationary (OD = 1.5) phase. The number of cells collected
486 was kept constant for each growth phase. Total RNA was extracted, DNA and rRNA were removed, and
487 libraries constructed and sequenced as detailed in the Supplementary file: Material and Methods.
488 Three biological triplicates were prepared for each growth phase.
489 A complete analysis of the RNA-Seq results will be the subject of a subsequent report. For this report
490 the numbers of RNA-Seq reads for each condition were first normalized to the number of reads
491 mapped to the gene *holD*, which was determined by rtPCR to be expressed at the same level in all
492 phases of growth. The means of the normalized RNA reads from the triplicates were then binned into
493 the same bins used for the mutational analysis. A fourth-order Daubechies wavelet transform was
494 performed on the binned RNA-Seq reads as described for the mutational data (1).

495 **Statistical Analysis**

496 To obtain the BPS density patterns, the numbers of BPSs were binned into 46 bins, each 100 Kb long, as
497 described (1). A fourth-order Daubechies wavelet transform was performed on the binned mutation
498 data as described (1). For presentation in the figures, these results were converted into rates by
499 dividing the number of BPS by the appropriate number of generations. Pearson's product-moment
500 correlation coefficient, ρ, was used to evaluate the correlations between the binned BPS data (Table

1). Spearman's nonparametric correlation coefficient was also computed for a few data sets, but gave similar results. To account for multiple comparisons, p values were adjusted using the Benjamini-Hochberg method (71) with the false discovery rate set at 25%, implemented with the MatLab R2018a "mafdr" command. Because comparisons using the data from the same strain are not independent, this adjustment was made separately for each column in Tables 1 and 2.

To further compare the BPS density patterns between two data sets, wavelet coherence was calculated and plotted using the MatLab R2018a "wcoherence" command. While the Daubechies wavelet provides a good visual representation of the binned data, it is not continuous and thus not easily adapted for wavelet coherence analysis. The MatLab program first converts the binned data to Morlet wavelets and then computes the coherence between two of these wavelets. We chose to analyze the data with wavelet coherence because it gives a measure of the correlation between the signals (displayed as colors in the figures) (72, 73). In addition, the MatLab wavelet coherence plot indicates, as a dashed curve, the 'cone of influence' within which results are free of artifactual edge effects (72). The relative phase-lag between the two signals is indicated by small arrows: arrows pointing right indicate in-phase, arrows pointing left indicate 180° out-of-phase, and arrows pointing in other directions indicate the various degrees in between. Because the MatLab program assumes a frequency-time series, the X axis of the plot is cycles/sample and the Y axis is time; we converted these to bins/cycle (on an inverted scale) and bins, respectively.

Declarations

Ethics approval and consent to participate: Not applicable

Consent for publication: Not applicable

522 **Availability of data and material**

523 The sequences and SNPs reported in this paper have been deposited with the National Center for
524 Biotechnology Information Sequence Read Archive https://trace.ncbi.nlm.nih.gov/Traces/sra/
525 (accession no. in progress) and in the IUScholarWorks Repository (hdl.handle.net/2022/20340).
526 Bacterial strains are available upon request

527 **Competing interests**

528 The authors declare no competing interests

529 **Funding**

530 This research was supported by US Army Research Office Multidisciplinary University Research
531 Initiative (MURI) Award W911NF-09-1-0444 to P.L.F. and H.T., the National Institutes of Health T32
532 GM007757 to B.A.N., and the US Army Undergraduate Research Apprenticeship Program to J. H. and S.
533 R

534 **Authors' contributions**

535 B.A.N. and P.L.F. designed the research, analyzed the data, and wrote the paper. B.A.N executed the
536 experiments. W.M., H.L., and H.T. performed the bioinformatic analyses. P.L.F. and H.T. supplied
537 resources. All authors read and approved the final manuscript.

538 **Acknowledgements**

539 We thank H. Bedwell-Ivers, C. Coplen, M. Durham, J. Eagan, N. Gruenhagen, J. A. Healy, N. Ivers,
540 C. Klineman., H. Lee, E. Popodi, I. Rameses, S. Riffert, H. Rivera, D. Simon, K. Smith, J. Townes, L. Tran,
541 and L. Whitson for technical help. Bacterial strains were kindly provided by R. Schaaper, R. Reyes-
542 Lamothe, D. Kearns, M. Konkol, and The National BioResource Project at the (Japanese) National
543 Institute of Genetics. We also thank S. E.Bell and X. Wang for technical help and discussions.

544 **References**

545 1. Foster PL, Hanson AJ, Lee H, Popodi EM, Tang H. On the mutational topology of the bacterial
546 genome. G3 (Bethesda). 2013;3(3):399-407.

547 2. Dillon MM, Sung W, Lynch M, Cooper VS. Periodic variation of mutation rates in bacterial
548 genomes associated with replication timing. MBio. 2018;9(4).

549 3. Dillon MM, Sung W, Sebra R, Lynch M, Cooper VS. Genome-wide biases in the rate and molecular
550 spectrum of spontaneous mutations in *Vibrio cholerae* and *Vibrio fischeri*. Mol Biol Evol. 2017;34(1):93-
551 109.

552 4. Wei W, Xiong L, Ye YN, Du MZ, Gao YZ, Zhang KY, et al. Mutation landscape of base substitutions,
553 duplications, and deletions in the representative current cholera pandemic strain. Genome Biol Evol.
554 2018;10(8):2072-85.

555 5. Long H, Sung W, Miller SF, Ackerman MS, Doak TG, Lynch M. Mutation rate, spectrum, topology,
556 and context-dependency in the DNA mismatch repair-deficient Pseudomonas fluorescens ATCC948.
557 Genome Biol Evol. 2014;7(1):262-71.

558 6. Dettman JR, Sztepanacz JL, Kassen R. The properties of spontaneous mutations in the
559 opportunistic pathogen Pseudomonas aeruginosa. BMC Genomics. 2016;17:27.

560 7. Lee H, Popodi E, Tang H, Foster PL. Rate and molecular spectrum of spontaneous mutations in
561 the bacterium *Escherichia coli* as determined by whole-genome sequencing. Proceedings of the
562 National Academy of Sciences of the United States of America. 2012;109(41):E2774-E83.

563 8. Marinus MG. DNA Mismatch Repair. EcoSal Plus. 2012; doi:10.1128/ecosalplus.7.2.5

564 9. Ganai RA, Johansson E. DNA replication-a matter of fidelity. Mol Cell. 2016;62(5):745-55.

565 10. Niccum BA, Lee H, MohammedIsmail W, Tang H, Foster PL. The spectrum of replication errors in
566 the absence of error correction assayed across the whole genome of *Escherichia coli*. Genetics.
567 2018;209(4):1043-54.
568 11. Foster PL, Niccum BA, Popodi E, Townes JP, Lee H, MohammedIsmail W, et al. Determinants of
569 base-pair substitution patterns revealed by whole-genome sequencing of DNA mismatch repair
570 defective *Escherichia coli*. Genetics. 2018;209(4):1029-42.
571 12. Valens M, Penaud S, Rossignol M, Cornet F, Boccard F. Macrodomain organization of the
572 *Escherichia coli* chromosome. EMBO J. 2004;23(21):4330-41.
573 13. Jinks-Robertson S, Bhagwat AS. Transcription-associated mutagenesis. Annu Rev Genet.
574 2014;48:341-59.
575 14. Rasouly A, Pani B, Nudler E. A magic spot in genome maintenance. Trends Genet. 2017;33(1):58-
576 67.
577 15. Zhang X, Zhang X, Zhang X, Liao Y, Song L, Zhang Q, et al. Spatial vulnerabilities of the *Escherichia*
578 *coli* genome to spontaneous mutations revealed with improved duplex sequencing. Genetics.
579 2018;210(2):547-58.
580 16. Withey JH, Friedman DI. A salvage pathway for protein structures: tmRNA and trans-translation.
581 Annu Rev Microbiol. 2003;57:101-23.
582 17. Kogoma T. Stable DNA replication: interplay between DNA replication, homologous
583 recombination, and transcription. Microbioland MolecBiolRev. 1997;61:212-38.
584 18. Maduike NZ, Tehranchi AK, Wang JD, Kreuzer KN. Replication of the *Escherichia coli* chromosome
585 in RNase HI-deficient cells: multiple initiation regions and fork dynamics. Mol Microbiol. 2014;91(1):39-
586 56.

587 19. Wang X, Lesterlin C, Reyes-Lamothe R, Ball G, Sherratt DJ. Replication and segregation of an
588 *Escherichia coli* chromosome with two replication origins. Proceedings of the National Academy of
589 Sciences of the United States of America. 2011;108(26):E243-50.
590 20. Ivanova D, Taylor T, Smith SL, Dimude JU, Upton AL, Mehrjouy MM, et al. Shaping the landscape
591 of the *Escherichia coli* chromosome: replication-transcription encounters in cells with an ectopic
592 replication origin. Nucleic Acids Res. 2015;43(16):7865-77.
593 21. Waldminghaus T, Skarstad K. The *Escherichia coli* SeqA protein. Plasmid. 2009;61(3):141-50.
594 22. Sutera VA, Jr., Lovett ST. The role of replication initiation control in promoting survival of
595 replication fork damage. MolMicrobiol. 2006;60(1):229-39.
596 23. Sanchez-Romero MA, Busby SJ, Dyer NP, Ott S, Millard AD, Grainger DC. Dynamic distribution of
597 SeqA protein across the chromosome of *Escherichia coli* K-12. MBio. 2010;1(1):e00012-10.
598 24. Weitao T, Nordstrom K, Dasgupta S. *Escherichia coli* cell cycle control genes affect chromosome
599 superhelicity. EMBO Rep. 2000;1(6):494-9.
600 25. Lobner-Olesen A, Marinus MG, Hansen FG. Role of SeqA and Dam in *Escherichia coli* gene
601 expression: a global/microarray analysis. Proceedings of the National Academy of Sciences of the
602 United States of America. 2003;100(8):4672-7.
603 26. Waldminghaus T, Skarstad K. ChIP on Chip: surprising results are often artifacts. BMC Genomics.
604 2010;11:414.
605 27. Sun L, Fuchs JA. *Escherichia coli* ribonucleotide reductase expression is cell cycle regulated. Mol
606 Biol Cell. 1992;3(10):1095-105.

607 28. Gon S, Camara JE, Klungsoyr HK, Crooke E, Skarstad K, Beckwith J. A novel regulatory mechanism
608 couples deoxyribonucleotide synthesis and DNA replication in *Escherichia coli*. EMBO J.
609 2006;25(5):1137-47.
610 29. Cooper S, Helmstetter CE. Chromosome replication and the division cycle of *Escherichia coli* B/r. J
611 Mol Biol. 1968;31(3):519-40.
612 30. Claret L, Rouviere-Yaniv J. Variation in HU composition during growth of *Escherichia coli*: the
613 heterodimer is required for long term survival. J Mol Biol. 1997;273(1):93-104.
614 31. Dorman CJ. Function of nucleoid-associated proteins in chromosome structuring and
615 transcriptional regulation. J Mol Microbiol Biotechnol. 2014;24(5-6):316-31.
616 32. Kahramanoglou C, Seshasayee AS, Prieto AI, Ibberson D, Schmidt S, Zimmermann J, et al. Direct
617 and indirect effects of H-NS and Fis on global gene expression control in *Escherichia coli*. Nucleic Acids
618 Res. 2011;39(6):2073-91.
619 33. Torrents E, Grinberg I, Gorovitz-Harris B, Lundstrom H, Borovok I, Aharonowitz Y, et al. NrdR
620 controls differential expression of the *Escherichia coli* ribonucleotide reductase genes. J Bacteriol.
621 2007;189(14):5012-21.
622 34. Lane HE, Denhardt DT. The rep mutation. IV. Slower movement of replication forks in *Escherichia*
623 *coli* rep strains. J Mol Biol. 1975;97(1):99-112.
624 35. Guy CP, Atkinson J, Gupta MK, Mahdi AA, Gwynn EJ, Rudolph CJ, et al. Rep provides a second
625 motor at the replisome to promote duplication of protein-bound DNA. Mol Cell. 2009;36(4):654-66.
626 36. Boubakri H, de Septenville AL, Viguera E, Michel B. The helicases DinG, Rep and UvrD cooperate
627 to promote replication across transcription units in vivo. EMBO J. 2010;29(1):145-57.

628 37. Myka KK, Hawkins M, Syeda AH, Gupta MK, Meharg C, Dillingham MS, et al. Inhibiting translation
629 elongation can aid genome duplication in *Escherichia coli*. Nucleic Acids Res. 2017;45(5):2571-84.
630 38. Heller RC, Marians KJ. Non-replicative helicases at the replication fork. DNA Repair (Amst).
631 2007;6(7):945-52.
632 39. Sandler SJ, Marians KJ. Role of PriA in replication fork reativation in *Escherichia coli*. J Bact.
633 2000;182:9-13.
634 40. Duggin IG, Wake RG, Bell SD, Hill TM. The replication fork trap and termination of chromosome
635 replication. MolMicrobiol. 2008;70(6):1323-33.
636 41. Mercier R, Petit MA, Schbath S, Robin S, El Karoui M, Boccard F, et al. The MatP/matS site-specific
637 system organizes the terminus region of the *E. coli* chromosome into a macrodomain. Cell.
638 2008;135(3):475-85.
639 42. Espeli O, Borne R, Dupaigne P, Thiel A, Gigant E, Mercier R, et al. A MatP-divisome interaction
640 coordinates chromosome segregation with cell division in *E. coli*. EMBO J. 2012;31(14):3198-211.
641 43. Syeda AH, Hawkins M, McGlynn P. Recombination and replication. Cold Spring Harb Perspect
642 Biol. 2014;6(11):a016550.
643 44. Louarn JM, Louarn J, Francois V, Patte J. Analysis and possible role of hyperrecombination in the
644 termination region of the *Escherichia coli* chromosome. J Bacteriol. 1991;173(16):5097-104.
645 45. Bierne H, Ehrlich SD, Michel B. The replication termination signal terB of the *Escherichia coli*
646 chromosome is a deletion hot spot. EMBO J. 1991;10(9):2699-705.
647 46. Louarn J, Cornet F, Francois V, Patte J, Louarn JM. Hyperrecombination in the terminus region of
648 the *Escherichia coli* chromosome: possible relation to nucleoid organization. J Bacteriol.
649 1994;176(24):7524-31.

650 47. Corre J, Cornet F, Patte J, Louarn JM. Unraveling a region-specific hyper-recombination
651 phenomenon: genetic control and modalities of terminal recombination in *Escherichia coli*. Genetics.
652 1997;147(3):979-89.
653 48. Cox MM. Regulation of bacterial RecA protein function. Crit Rev Biochem Mol Biol.
654 2007;42(1):41-63.
655 49. Little JW, Harper JE. Identification of the lexA gene product of *Escherichia coli* K-12. Proceedings
656 of the National Academy of Sciences of the United States of America. 1979;76(12):6147-51.
657 50. Prieto AI, Kahramanoglou C, Ali RM, Fraser GM, Seshasayee AS, Luscombe NM. Genomic analysis
658 of DNA binding and gene regulation by homologous nucleoid-associated proteins IHF and HU in
659 *Escherichia coli* K12. Nucleic Acids Res. 2012;40(8):3524-37.
660 51. Sobetzko P, Travers A, Muskhelishvili G. Gene order and chromosome dynamics coordinate
661 spatiotemporal gene expression during the bacterial growth cycle. ProcNatlAcadSciUSA.
662 2012;109(2):E42-E50.
663 52. Cho BK, Knight EM, Barrett CL, Palsson BO. Genome-wide analysis of Fis binding in *Escherichia*
664 *coli* indicates a causative role for A-/AT-tracts. Genome Res. 2008;18(6):900-10.
665 53. Wang W, Li GW, Chen C, Xie XS, Zhuang X. Chromosome organization by a nucleoid-associated
666 protein in live bacteria. Science. 2011;333(6048):1445-9.
667 54. Lang B, Blot N, Bouffartigues E, Buckle M, Geertz M, Gualerzi CO, et al. High-affinity DNA binding
668 sites for H-NS provide a molecular basis for selective silencing within proteobacterial genomes. Nucleic
669 Acids Res. 2007;35(18):6330-7.

670 55. Bouffartigues E, Buckle M, Badaut C, Travers A, Rimsky S. H-NS cooperative binding to high-
671 affinity sites in a regulatory element results in transcriptional silencing. Nat Struct Mol Biol.
672 2007;14(5):441-8.
673 56. Wolf SG, Frenkiel D, Arad T, Finkel SE, Kolter R, Minsky A. DNA protection by stress-induced
674 biocrystallization. Nature. 1999;400(6739):83-5.
675 57. Foster PL, Lee H, Popodi E, Townes JP, Tang H. Determinants of spontaneous mutation in the
676 bacterium *Escherichia coli* as revealed by whole-genome sequencing. Proceedings of the National
677 Academy of Sciences of the United States of America. 2015;112(44):E5990-E599.
678 58. Duigou S, Boccard F. Long range chromosome organization in *Escherichia coli*: The position of the
679 replication origin defines the non-structured regions and the Right and Left macrodomains. PLoS
680 Genet. 2017;13(5):e1006758.
681 59. Dupaigne P, Tonthat NK, Espeli O, Whitfill T, Boccard F, Schumacher MA. Molecular basis for a
682 protein-mediated DNA-bridging mechanism that functions in condensation of the *E. coli* chromosome.
683 Mol Cell. 2012;48(4):560-71.
684 60. Lioy VS, Cournac A, Marbouty M, Duigou S, Mozziconacci J, Espeli O, et al. Multiscale structuring
685 of the *E. coli* chromosome by nucleoid-associated and condensin proteins. Cell. 2018;172(4):771-83
686 e18.
687 61. Thiel A, Valens M, Vallet-Gely I, Espeli O, Boccard F. Long-range chromosome organization in *E.*
688 *coli*: a site-specific system isolates the Ter macrodomain. PLoSGenet. 2012;8(4):e1002672.
689 62. Salgado H, Peralta-Gil M, Gama-Castro S, Santos-Zavaleta A, Muniz-Rascado L, Garcia-Sotelo JS, et
690 al. RegulonDB v8.0: omics data sets, evolutionary conservation, regulatory phrases, cross-validated
691 gold standards and more. Nucleic Acids Res. 2013;41(Database issue):D203-13.

692 63. Guo F, Adhya S. Spiral structure of *Escherichia coli* HUalphabeta provides foundation for DNA
693 supercoiling. Proceedings of the National Academy of Sciences of the United States of America.
694 2007;104(11):4309-14.
695 64. van Noort J, Verbrugge S, Goosen N, Dekker C, Dame RT. Dual architectural roles of HU:
696 formation of flexible hinges and rigid filaments. Proceedings of the National Academy of Sciences of
697 the United States of America. 2004;101(18):6969-74.
698 65. Pinson V, Takahashi M, Rouviere-Yaniv J. Differential binding of the *Escherichia coli* HU,
699 homodimeric forms and heterodimeric form to linear, gapped and cruciform DNA. J Mol Biol.
700 1999;287(3):485-97.
701 66. Bonnefoy E, Almeida A, Rouviere-Yaniv J. Lon-dependent regulation of the DNA binding protein
702 HU in *Escherichia coli*. Proceedings of the National Academy of Sciences of the United States of
703 America. 1989;86(20):7691-5.
704 67. Berger M, Farcas A, Geertz M, Zhelyazkova P, Brix K, Travers A, et al. Coordination of genomic
705 structure and transcription by the main bacterial nucleoid-associated protein HU. EMBO Rep.
706 2010;11(1):59-64.
707 68. Browning DF, Grainger DC, Busby SJ. Effects of nucleoid-associated proteins on bacterial
708 chromosome structure and gene expression. CurrOpinMicrobiol. 2010;13(6):773-80.
709 69. Grainger DC, Hurd D, Goldberg MD, Busby SJ. Association of nucleoid proteins with coding and
710 non-coding segments of the *Escherichia coli* genome. Nucleic Acids Res. 2006;34(16):4642-52.
711 70. Blot N, Mavathur R, Geertz M, Travers A, Muskhelishvili G. Homeostatic regulation of
712 supercoiling sensitivity coordinates transcription of the bacterial genome. EMBO Rep. 2006;7(7):710-5.

71. Benjamini Y, Hochberg Y. Controlling the false discovery rate - a practical and powerful approach to multiple testing. J Roy Stat Soc Ser B (Stat Method). 1995;57(1):289-300.

72. Grinsted A, Moore JC, Jevrejeva S. Application of the cross wavelet transform and wavelet coherence to geophysical time series. Nonlinear Processes in Geophysics. 2004;11:561-6.

73. Maraun D, Kurths J. Cross wavelet analysis: significance testing and pitfalls. Nonlinear Processes in Geophysics. 2004;11:505-14.

Table 1. Pearson's correlation, ρ, of each strain versus MMR⁻

		Whole Chromosome Bins 1 to 46		Right Replichore Bins 1 to 23		Left Replichore Bins 46 to 24		Origin Bins 1 to 13, 46 to 34		Terminus Bins 14 to 33	
Strain	Description	ρ	P[a]	ρ	P[a]	ρ	P[a]	ρ	P[a]	ρ	P[a]
Collective[b]	MMR⁻	—	—	—	—	—	—	—	—	—	—
Collective	MMR⁻ minus A:T ts at NAC/NTG	0.94	<0.001	0.93	<0.001	0.96	<0.001	0.97	<0.001	0.71	0.004
PFM421	Δ*rnhA* Δ*mutL*	0.74	<0.001	0.63	0.002	0.84	<0.001	0.81	<0.001	0.47	0.075
PFM669	Δ*mutL* (AB1157)	0.59	<0.001	0.40	0.064	0.75	<0.001	0.71	<0.001	0.45	0.079
PFM430/ 431	*oriC*⁺ *oriZ*⁺ Δ*mutL* (AB1157)	0.75	<0.001	0.71	<0.001	0.81	<0.001	0.83	<0.001	0.46	0.075
PFM426	Δ*oriC oriZ*⁺ Δ*mutL* (AB1157)	0.39	0.008	0.21	0.34	0.62	0.003	0.40	0.044	0.41	0.11
PFM533/ 534	Δ*seqA* Δ*mutL*	0.49	0.001	0.71	<0.001	0.27	0.23	0.53	0.006	0.38	0.14
PFM5[b]	Δ*mutL* on minimal medium	0.50	0.001	0.40	0.069	0.61	0.003	0.57	0.003	0.58	0.029

PFM343[b]	Δ*mutS* on minimal medium	0.18	0.22	0.18	0.41	0.18	0.41	0.21	0.31	0.22	0.38
PFM343[b]	Δ*mutS* on diluted LB	0.84	<0.001	0.84	<0.001	0.85	<0.001	0.87	<0.001	0.71	0.004
PFM343[b]	Δ*mutS* on supplemented minimal medium	0.81	<0.001	0.82	<0.001	0.81	<0.001	0.83	<0.001	0.65	0.008
PFM342[b]	Δ*mutS* at low temperature	0.57	<0.001	0.60	0.003	0.53	0.013	0.69	<0.001	-0.02	0.95
PFM799	Δ*nrdR* Δ*mutL*	0.49	0.001	0.58	0.005	0.39	0.080	0.69	<0.001	-0.31	0.24
PFM677	Δ*rep* Δ*mutL*	0.48	0.001	0.49	0.022	0.48	0.027	0.62	0.001	-0.12	0.67
PFM256	Δ*tus* Δ*mutL*	0.82	<0.001	0.79	<0.001	0.85	<0.001	0.87	<0.001	0.70	0.004
PFM257	Δ*matP* Δ*mutL*	0.40	0.007	0.60	0.004	0.21	0.34	0.70	<0.001	-0.47	0.075
PFM422	Δ*recA* Δ*mutL*	0.71	<0.001	0.70	<0.001	0.73	<0.001	0.85	<0.001	0.06	0.84
PFM424	Δ*recA* Δ*mutS*	0.80	<0.001	0.78	<0.001	0.83	<0.001	0.91	<0.001	0.44	0.082
PFM456	Δ*recB* Δ*mutL*	0.82	<0.001	0.87	<0.001	0.79	<0.001	0.89	<0.001	0.39	0.12
PFM118	Δ*umuDC* Δd*inB* Δ*mutL*	0.59	<0.001	0.62	0.003	0.55	0.010	0.61	0.001	0.69	0.004
PFM120	*lexA3* Δ*sulA* Δ*mutL*	0.82	<0.001	0.82	<0.001	0.83	<0.001	0.83	<0.001	0.80	0.001
PFM259	Δ*hupB* Δ*mutL*	0.73	<0.001	0.70	<0.001	0.77	<0.001	0.81	<0.001	0.57	0.031
PFM258	Δ*hupA* Δ*mutL*	0.49	0.001	0.43	0.053	0.58	0.005	0.67	<0.001	-0.23	0.38
PFM317/ 318	Δ*fis* Δ*mutL*	0.51	<0.001	0.61	0.003	0.42	0.060	0.67	<0.001	-0.30	0.25
PFM482	Δ*fis* Δ*mutS*	0.49	0.001	0.31	0.15	0.62	0.003	0.65	<0.001	-0.28	0.27

PFM741	Δ*hns* Δ*mutL*	0.81	<0.001	0.81	<0.001	0.81	<0.001	0.88	<0.001	0.46	0.075
PFM713	Δ*dps* Δ*mutL*	0.80	<0.001	0.84	<0.001	0.78	<0.001	0.89	<0.001	0.47	0.075
PFM163[c]	*mutD5*	0.76	<0.001	0.79	<0.001	0.74	<0.001	0.82	<0.001	0.78	0.001
PFM165/397/399[c]	*mutD5* Δ*mutL*	0.64	<0.001	0.76	<0.001	0.52	0.014	0.86	<0.001	-0.46	0.075
Collective[b]	Wild type	0.36	0.014	0.41	0.061	0.31	0.17	0.37	0.065	0.51	0.060
Collective[d]	*Bacillus subtilis* *mutS::*Tn*10*	0.52	<0.001	0.63	0.003	0.40	0.068	0.74	<0.001	-0.52	0.055

[a] P values were adjusted for multiple comparisons using the Benjamini-Hochberg method (71) with the false discovery rate set at 25%

[b] Data are from (11)

[c] Data are from (10)

[d] Data are combined from four MA experiments with DK2140 (NCIB3610 *mutS*::Tn*10*), DK2141 (NCIB3610 *mutS*::Tn*10*), DK2142 (NCIB3610 *mutS*::Tn*10* Δ*comI*), and DK2143 (NCIB3610 *mutS*::Tn*10* Δ*com*I). There were no differences in mutation rates or spectra among these strain

Table 2. Pearson's correlation, ρ, of right versus left replichore for each strain

		Whole Chromosome		Origin		Terminus	
		Bins 1 to 23, 46 to 24		Bins 1 to 13, 46 to 34		Bins 14 to 23, 33 to 24	
Strain	Description	ρ	P[a]	ρ	P[a]	ρ	P[a]
Collective[b]	MMR⁻	0.91	<0.001	0.95	<0.001	0.66	0.23
Collective	MMR⁻ minus A:T ts at NAC/NTG	0.89	<0.001	0.94	<0.001	0.42	0.60
PFM421	Δ*rnhA* Δ*mutL*	0.49	0.026	0.58	0.051	0.24	0.82
PFM669	Δ*mutL* (AB1157)	0.52	0.018	0.64	0.026	0.29	0.77
PFM430/ 431	*oriC*⁺ *oriZ*⁺ Δ*mutL* (AB1157)	0.60	0.005	0.80	0.003	0.19	0.84
PFM426	Δ*oriC oriZ*⁺ Δ*mutL (AB1157)*	0.28	0.22	0.33	0.31	-0.06	0.91
PFM533/ 534	Δ*seqA* Δ*mutL*	0.41	0.062	0.53	0.079	0.32	0.71
PFM5[b]	Δ*mutL* on minimal medium	0.27	0.22	0.19	0.53	0.05	0.91
PFM343[b]	Δ*mutS* on minimal medium	-0.02	0.93	0.32	0.31	-0.53	0.39
PFM343[b]	Δ*mutS* on diluted LB	0.87	<0.001	0.93	<0.001	0.66	0.23
PFM343[b]	Δ*mutS* on supplemented minimal medium	0.74	<0.001	0.79	0.003	0.54	0.39
PFM342[b]	Δ*mutS* at low temperature	0.84	<0.001	0.89	<0.001	0.73	0.19
PFM799	Δ*nrdR* Δ*mutL*	0.79	<0.001	0.78	0.003	0.84	0.07
PFM677	Δ*rep* Δ*mutL*	0.43	0.053	0.58	0.051	-0.16	0.84
PFM256	Δ*tus* Δ*mutL*	0.70	0.001	0.88	<0.001	0.26	0.81
PFM257	Δ*matP* Δ*mutL*	0.45	0.042	0.40	0.20	0.72	0.19

PFM422	Δ*recA* Δ*mutL*	0.66	0.001	0.81	0.003	0.11	0.88
PFM424	Δ*recA* Δ*mutS*	0.64	0.002	0.80	0.003	0.07	0.91
PFM456	Δ*recB* Δ*mutL*	0.67	0.001	0.78	0.003	0.03	0.94
PFM118	Δ*umuDC* Δ*dinB* Δ*mutL*	0.39	0.075	0.68	0.018	-0.13	0.87
PFM120	*lexA3* Δ*sulA* Δ*mutL*	0.51	0.019	0.57	0.055	0.42	0.60
PFM259	Δ*hupB* Δ*mutL*	0.64	0.002	0.78	0.003	0.35	0.65
PFM258	Δ*hupA* Δ*mutL*	0.54	0.014	0.69	0.015	0.15	0.84
PFM317/ 318	Δ*fis* Δ*mutL*	0.61	0.004	0.67	0.019	0.58	0.34
PFM482	Δ*fis* Δ*mutS*	0.34	0.13	0.49	0.108	0.19	0.84
PFM741	Δ*hns* Δ*mutL*	0.81	<0.001	0.85	0.001	0.60	0.33
PFM713	Δ*dps* Δ*mutL*	0.52	0.017	0.77	0.004	-0.20	0.84
PFM163[c]	*mutD5*	0.75	<0.001	0.77	0.004	0.52	0.39
PFM165/397/399[c]	*mutD5* Δ*mutL*	0.78	<0.001	0.88	<0.001	0.39	0.62
Collective[b]	Wild type	0.17	0.46	0.24	0.45	0.17	0.84
Collective[d]	*Bacillus subtilis mutS::*Tn*10*	0.73	<0.001	0.87	0.000	0.37	0.65

[a] P values were adjusted for multiple comparisons using the Benjamini-Hochberg method (71) with the false discovery rate set at 25%

[b] Data are from (11)

[c] Data are from (10)

[d] Data are combined from four MA experiments with DK2140 (NCIB3610 *mutS*::Tn*10*), DK2141 (NCIB3610 *mutS*::Tn*10*), DK2142 (NCIB3610 *mutS*::Tn*10* Δ*comI*), and DK2143 (NCIB3610 *mutS*::Tn*10* Δ*com*I). There were no differences in mutation rates or spectra among these strain

Figure Legends

Figure 1. The BPS density pattern is not due to transcription but is affected by moving the origin of replication. For each plot the data were collected into 100 Kb bins starting at the origin of replication on the left and continuing clockwise around the chromosome back to the origin on the right. **Figure 1A**. The BPS density pattern of MMR-defective strains. Bars represent the mean mutation rate in each bin calculated from the BPSs collected from 10 experiments with MMR-defective strains. Error bars are the 95% CLs of the means. The grey line represents the Daubechies wavelet transform of the binned data. The chromosomal macrodomains (MCs) are indicated at the top of the plot: green, Ori MC; blue, Right and Left MC; red, Ter MC. **Figure 1B**. The Daubechies wavelet transform of the binned reads from RNA-Seq samples taken during lag, log, and stationary growth phases of the Δ*mutL* mutant strain, PFM144. The data used for the wavelet transforms were the means of three biological replicates. Arrows indicate the positions of the rRNA operons, but the reads from the ribosomal genes in those operons were not included in the plot. **Figure 1C, D, E, and F**. The BPS density patterns (bars) and Daubechies wavelet transforms (pink line) of the indicated mutant strains compared to the Daubechies wavelet transform of the combined MMR^{-} strains (grey line). See text for a description of the strains. In each plot the left-hand scale has been adjusted to bring the wavelets close together for comparison. The red arrow in 1E indicates the position of *oriZ*. Strains: 1C, PFM421; 1D, PFM430/431; 1E, PFM426; 1F, PFM533/534.

Figure 2. Altering the progression of DNA replication affects the BPS density pattern. For each plot the data were collected into 100 Kb bins starting at the origin of replication on the left and continuing clockwise around the chromosome back to the origin on the right. The BPS density

23 patterns (bars) and Daubechies wavelet transforms (pink lines) of the indicated strains are
24 compared to the Daubechies wavelet transform of the combined MMR⁻ strains (grey line). In
25 each plot the left-hand scale has been adjusted to bring the wavelets close together for
26 comparison. **Figure 2A, B, C, and D**. Altering the cellular growth rate by growing a Δ*mutS*
27 mutant strain on different medium and at different temperatures differentially affects the BPS
28 density pattern. In the experiments shown in Plot A, C, and D, the cells grew at about half the
29 normal rate, whereas in the experiment shown in plot B they grew at the normal rate. Strains:
30 2A, 2B, and 2C, PFM343; 2D, PFM342. **Figure 2E and F**. Dysregulation of dNTP levels and loss of
31 Rep, the auxiliary replication helicase, affect the BPS density pattern. 2E, PFM799; 2F, PFM677.
32 **Figure 2G and H**. Loss of the Tus antihelicase has no effect, but loss of the terminus organizing
33 protein, MatP, changes the BPS density pattern across the chromosome. The arrows in Figure
34 2G mark the major Ter sites where Tus binds. The bar in Figure 2H shows the region in which
35 MatP binds. Strains: 2G, PFM256; 2H, PFM257.
36 **Figure 3**. Loss of RecA, HUα, or Fis changes the BPS pattern, but the SOS response and loss of
37 other NAPs do not. For a description of the plots, see the legend to Figure 2. **Figure 3A, B, and**
38 **C.** Loss of RecA alters the BPS density pattern in the terminus region, but not through its role as
39 a master regulator of the SOS response. RecA (Figure 3A) is *E. coli*'s major recombinase. The
40 *dinB* and *umuDC* genes (Figure 3B) encode the error-prone DNA polymerases, Pol IV and Pol V,
41 that are induced as part of the SOS response. The *lexA3* allele encodes a non-inducible
42 repressor of the SOS genes. Deletion of *sulA* prevents lethal filamentation after induction of the
43 SOS response (not relevant to this study). Strains: 3A, PFM422; 3B, PFM118; 3C, PFM120.
44 **Figure 3D, E, F, G, and H.** Loss of the HUα subunit of HU or of Fis changes the BPS density

45 pattern, but loss of the HUβ subunit of HU, HNS, or DPS has only minor effects. Strains: 3D,

46 PFM259; 3E, PFM258; 3F, PFM317/318; 3G, PFM741/742; 3H, PFM713.

47 **Figure 4.** The BPS density pattern is a result of biased correction by replication proofreading

48 and MMR. For a description of the plots, see the legend to Figure 2. **Figure 4A and B**. A strain

49 with deficient proofreading but active MMR yields a BPS pattern similar to a MMR-defective

50 strain, but a strain with neither proofreading nor MMR does not. The *mutD5* allele encodes an

51 exonuclease deficient proofreader. Strains: 4A, PFM163; 4B, PFM165/397/399. **Figure 4C and**

52 **D.** The BPS density pattern in the wild-type strain does not match the pattern of either the

53 MMR-defective strain, or the *mutD5* mutant strain. The green line in Figure 1D is the

54 Daubechies wavelet transform of the *mutD5* mutant strain (pink line in Figure 4A). Strains: 4C

55 and D, eight strains with wild-type mutational phenotypes (see text). **Figure 4E**. MMR-defective

56 *B. subtilis* also has a symmetrical BPS density pattern, but it is different than *E. coli*'s pattern.

57 Strains: three *B. subtilis* mutant strains with the same mutational phenotype (see

58 supplementary Tables S1 and S3).

Figure 1

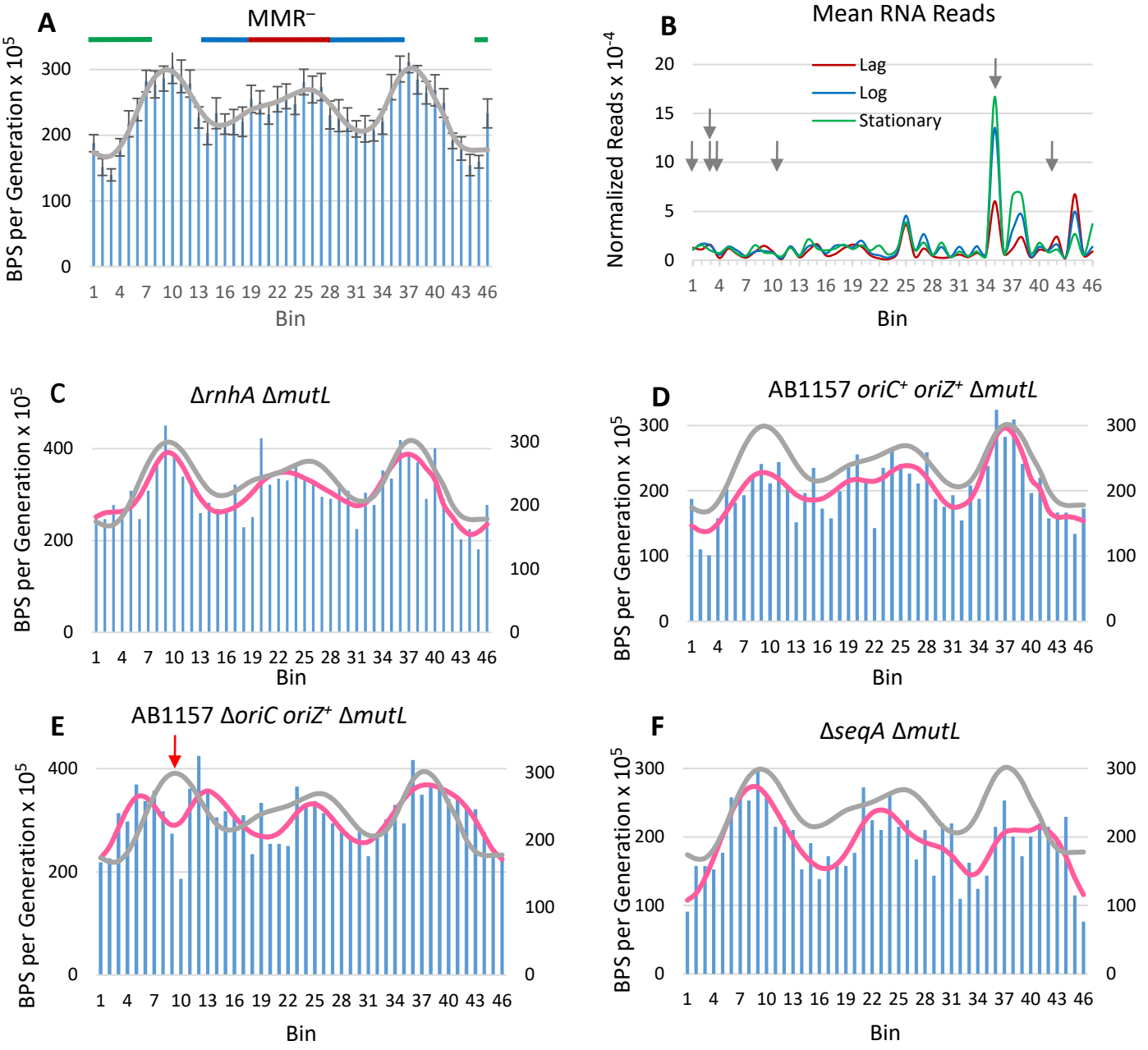
A
MMR⁻
BPS per Generation x 10^5
300
200
100
0
1 4 7 10 13 16 19 22 25 28 31 34 37 40 43 46
Bin
B
Mean RNA Reads
Normalized Reads x 10^-4
20
15
10
5
0
Lag
Log
Stationary
1 4 7 10 13 16 19 22 25 28 31 34 37 40 43 46
Bin
C
ΔrnhA ΔmutL
BPS per Generation x 10^5
400
200
0
300
200
100
0
1 4 7 10 13 16 19 22 25 28 31 34 37 40 43 46
Bin
D
AB1157 oriC⁺ oriZ⁺ ΔmutL
BPS per Generation x 10^5
300
200
100
0
300
200
100
0
1 4 7 10 13 16 19 22 25 28 31 34 37 40 43 46
Bin
E
AB1157 ΔoriC oriZ⁺ ΔmutL
BPS per Generation x 10^5
400
200
0
300
200
100
0
1 4 7 10 13 16 19 22 25 28 31 34 37 40 43 46
Bin
F
ΔseqA ΔmutL
BPS per Generation x 10^5
300
200
100
0
300
200
100
0
1 4 7 10 13 16 19 22 25 28 31 34 37 40 43 46
Bin

Figure 2

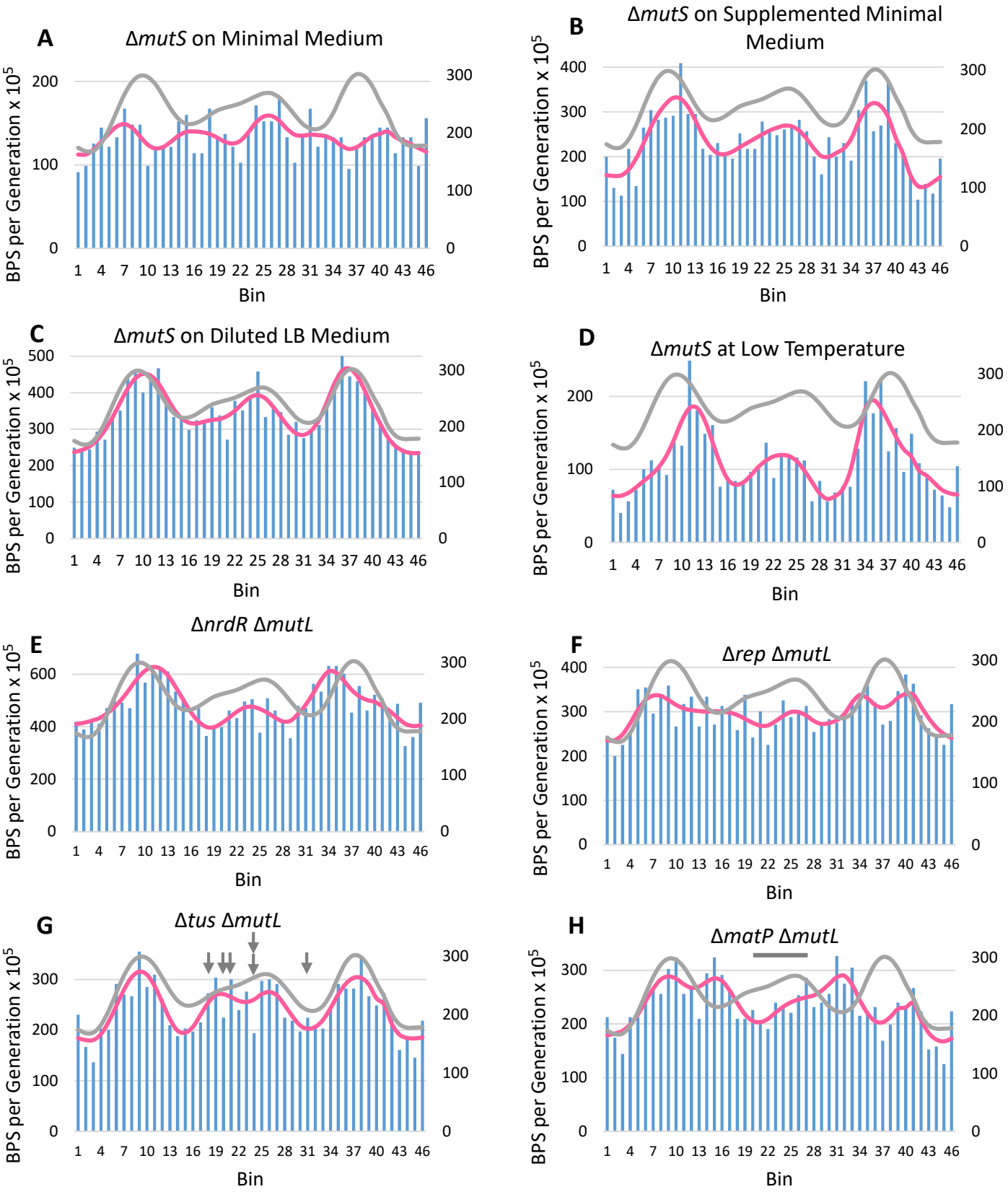
A
ΔmutS on Minimal Medium
B
ΔmutS on Supplemented Minimal Medium
C
ΔmutS on Diluted LB Medium
D
ΔmutS at Low Temperature
E
ΔnrdR ΔmutL
F
Δrep ΔmutL
G
Δtus ΔmutL
H
ΔmatP ΔmutL
BPS per Generation x 10^5
Bin
1 4 7 10 13 16 19 22 25 28 31 34 37 40 43 46

Figure 3

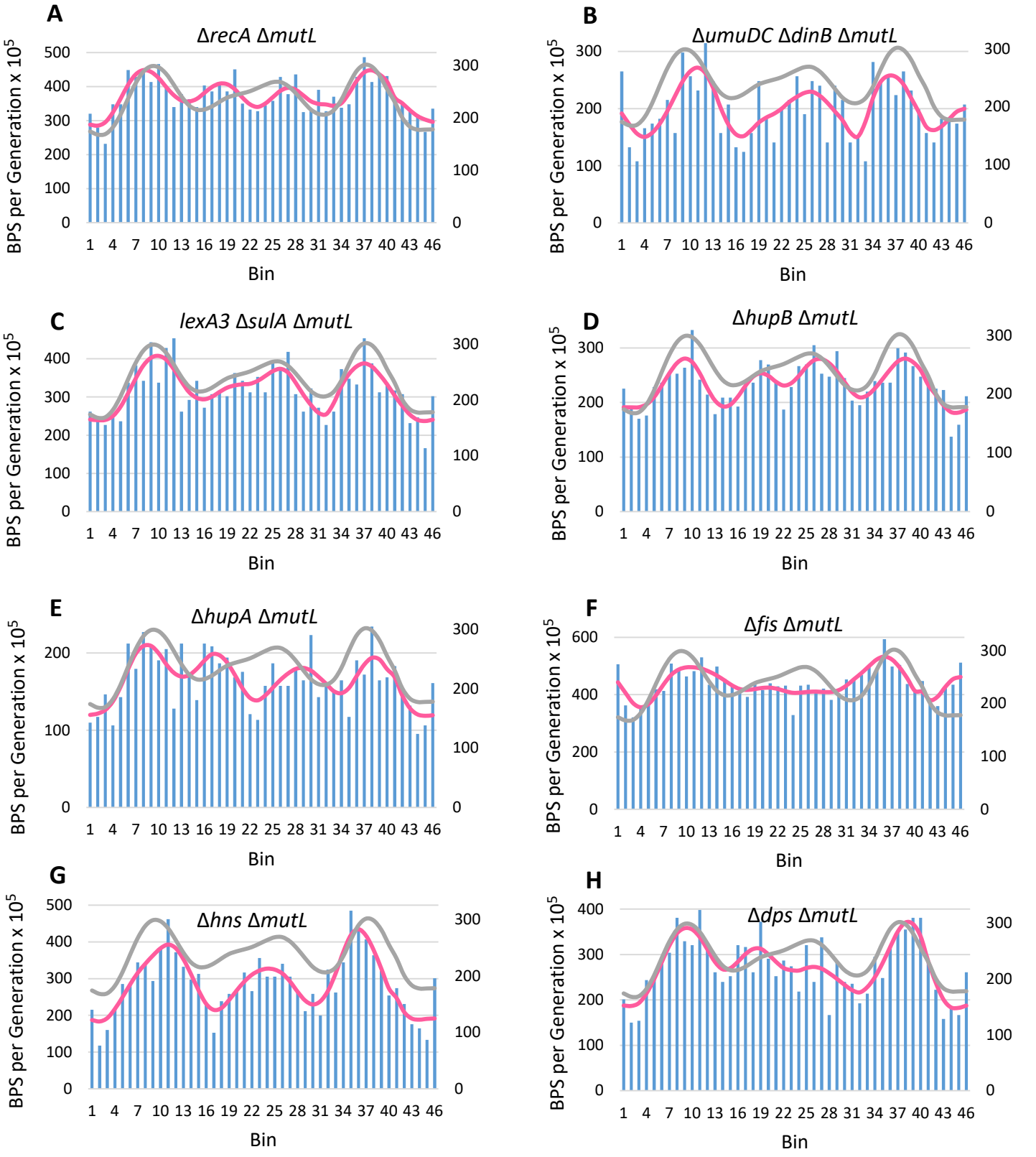
A
ΔrecA ΔmutL
B
ΔumuDC ΔdinB ΔmutL
C
lexA3 ΔsulA ΔmutL
D
ΔhupB ΔmutL
E
ΔhupA ΔmutL
F
Δfis ΔmutL
G
Δhns ΔmutL
H
Δdps ΔmutL
BPS per Generation x 10^5
Bin

Figure 4

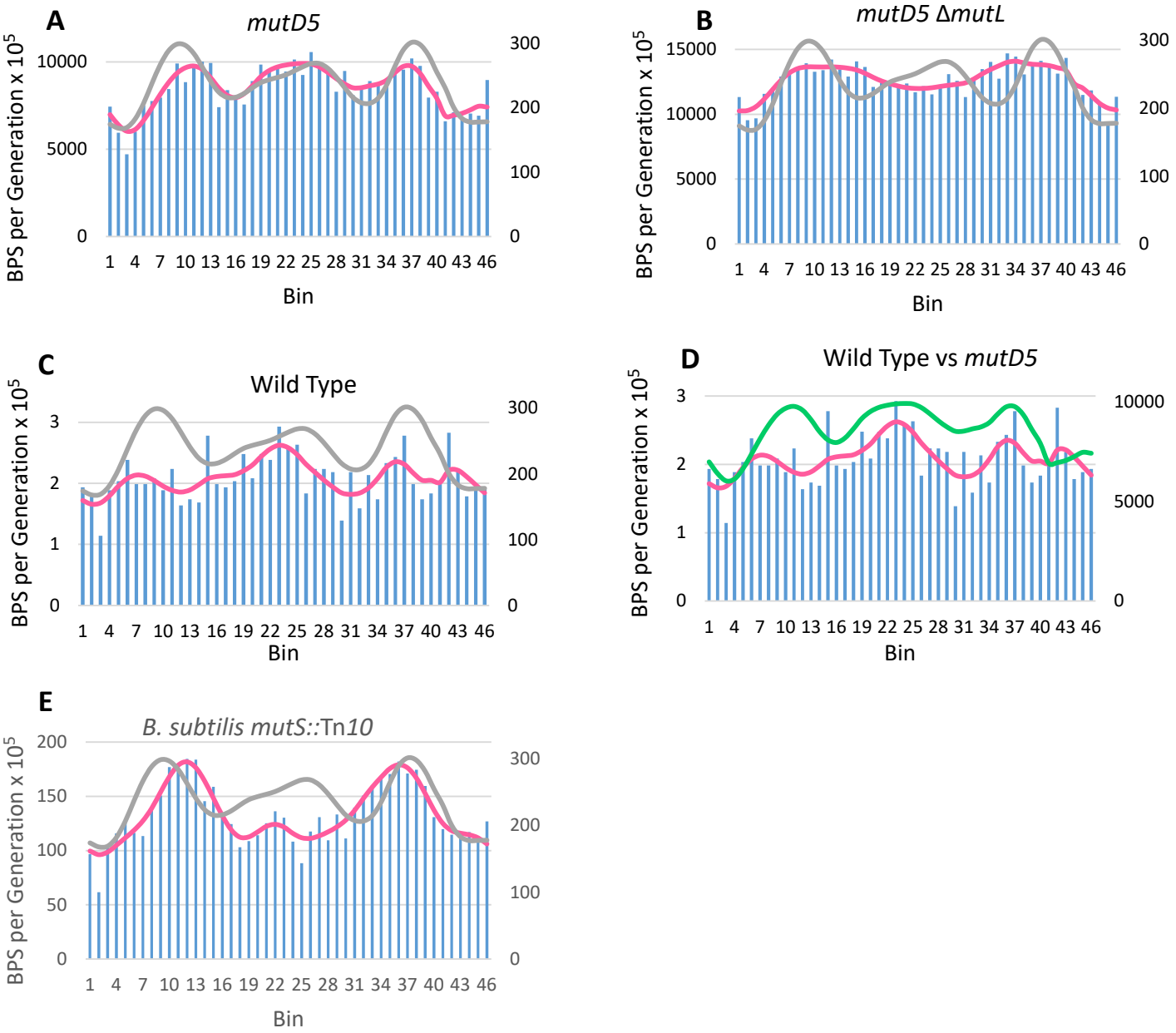
A
mutD5
BPS per Generation x 10^5
10000
5000
0
300
200
100
0
1 4 7 10 13 16 19 22 25 28 31 34 37 40 43 46
Bin
B
mutD5 ΔmutL
BPS per Generation x 10^5
15000
10000
5000
0
300
200
100
0
1 4 7 10 13 16 19 22 25 28 31 34 37 40 43 46
Bin
C
Wild Type
BPS per Generation x 10^5
3
2
1
0
300
200
100
0
1 4 7 10 13 16 19 22 25 28 31 34 37 40 43 46
Bin
D
Wild Type vs mutD5
BPS per Generation x 10^5
3
2
1
0
10000
5000
0
1 4 7 10 13 16 19 22 25 28 31 34 37 40 43 46
Bin
E
B. subtilis mutS::Tn10
BPS per Generation x 10^5
200
150
100
50
0
300
200
100
0
1 4 7 10 13 16 19 22 25 28 31 34 37 40 43 46
Bin

Supplemental Material and Methods

Bacterial strains and media

The strains used in this study are listed in Supplemental Table S1. All E. coli strains were derived from PFM2 (1) or AB1157 (2). The *oriC*$^+$ *oriZ*$^+$ and Δ*oriC oriZ*$^+$ strains were a gift from Rodrigo Reyes-Lamothe (McGill University). The *mutD5* allele was obtained from Roel Schaaper (NIEHS). The deletion mutations originated in the Keio collection (3) and were moved by P1 phage transduction (4); the Kn^r element was removed by using FLP recombination (5). The deletions were confirmed by PCR analysis using the oligonucleotides listed in Supplemental Table S2. The *B. subtilis* strains were derived from the undomesticated ancestral strain NCIB3610 and were a gift from M.A. Konkol and D.B. Kearns (Indiana University).

Rich medium was Miller Luria Broth (LB) (Difco; BD); minimal medium was Vogel-Bonner minimal medium (VB min) with 0.2% glucose (6). When required, antibiotic concentrations were: carbenicillin (Carb), 100 μg/ml; kanamycin (Kn), 50 μg/ml; nalidixic acid (Nal), 40 μg/ml; chloramphenicol (Cam), 30 μg/ml; and, rifampicin (Rif), 100 μg/ml. Half of these concentrations were used in minimal medium.

Estimation of mutation rates from fluctuation assays

Mutation rates were determined as described (7), using mutation to Nal^R or Rif^R. The Ma-Sandri-Sarkar maximum likelihood method was used to calculate the mutation rates by using the FALCOR web tool found at www.mitochondria.org/protocols/FALCOR.html (8).

Mutation accumulation experiments

The MA procedure has been described (1, 9, 10). The MA lines originated from single colonies isolated from a founder colony, obtained by streaking from a freezer stock onto agar plates of the medium to be used in the MA experiment. After incubation overnight at the experimental temperature, one well

23 isolated colony was excised from the agar plate, soaked for 30 minutes in 0.85% NACL + 0.01% gelatin,
24 and then vortexed for 60 seconds. Appropriate dilutions for obtaining well-isolated colonies were then
25 plated onto the appropriate agar plates at the appropriate temperature to start MA lines. Plates were
26 incubated at 37°C for most experiments, or at 28°C for the experiment at low temperature. Each MA
27 line was periodically streaked for a single colony: on LB and supplemented VB min agar plates at 37°C,
28 this was done daily; on VB min and diluted LB agar plates at 37°C, and on LB plates at 28°C, this was
29 done every 48 hours. The number of passes required was determined by the preliminary mutation rate
30 obtained from a fluctuation assay. The parameters of the MA experiment including the number of lines
31 used for each strain and the total number of generations per experiment are given in Supplemental
32 Table S3.

33 **Estimation of generations**

34 The method to estimate that number of generations undergone in each MA experiment is described (1,
35 9). The diameter of the single colonies streaked was recorded daily, and then the number of cells in
36 colonies of different diameters was determined for each experiment as described (1). The daily colony
37 diameters were converted to generations and the results summed.

38 **Genomic DNA preparation, library construction, and sequencing**

39 Genomic DNA was isolated using PureLink Genomic DNA purification kit (Invitrogen) from a
40 predetermined amount of overnight LB culture inoculated from the freezer stocks made after the last
41 passage of the MA line. DNA concentration was measured on an Epoch Microplate Spectrophotometer
42 (BioTek Instruments, Inc.). The identity of the lines was confirmed before library construction by
43 verifying the presence of the expected gene deletions in the gDNA with diagnostic PCR using the
44 oligonucleotides in Supplemental Table S2. Libraries were made by the Indiana University Center for

45 Genomics and Bioinformatics and were sequenced using the Illumina HiSeq 2500 platform at the
46 University of New Hampshire Hubbart Center for Genome Studies or the Illumina NextSeq platform at
47 the Indiana University Center for Genomics and Bioinformatics.

48 **Sequence analysis**

49 SNP calling is described (1). The reference genome used for *E. coli* was NCBI reference sequence
50 NC_000913.2, and for *B. subtilis* was GenBank: CP020102.1. The Illumina reads were aligned to the
51 referenced genomes using the Burrows-Wheeler short-read alignment tool, BWA version 0.7.9 (11).

52 Poor sequence coverage resulted in some MA lines being eliminated. Cross-contamination can
53 occur during streaking, resulting in lines with identical mutations. If two lines shared over 50% of their
54 mutations then one of the lines was dropped from further analysis. If lines shared less than 50%, then
55 each shared mutation was assigned to one of the lines and dropped from the others. If lineage could
56 be established the shared mutation was assigned accordingly, otherwise the mutation was assigned
57 randomly.

58 **RNA sequencing**

59 The *E. coli* strain PFM144, which is PFM2 Δ*mutL* (10), was grown in LB and aliquots collected during lag
60 (OD = 0.022), log (OD = 0.3), and stationary (OD = 1.5) phase.. The number of cells collected was kept
61 constant for each growth phase. Cells were pelleted at 10,000gs for 10 min, 1ml of medium was added
62 and the cells were pelleted again at 10,000gs for 2 min. The pellets were then flash frozen in liquid
63 nitrogen and stored at -80°. Three biological triplicates were prepared for each growth phase.

64 RNA was extracted using FastRNA Pro Blue kit (MP Biomedicals). DNA was removed by using
65 TurboDNase (Ambion). DNA removal was confirmed with diagnostic PCR using primer pair “fis forward”
66 and “fis reverse” (Supplemental Table S2). rRNA was removed using RiboMinus magnetic beads kit

67 (Invitrogen). RNA concentration and purity was assessed with an Epoch Microplate Spectrophotometer

68 (BioTek Instruments, Inc.). Libraries were made by the Indiana University CGB and were sequenced at

69 UT Health Science Center on Illumina HiSeq 2500 platform.

Table S1. Bacterial strains used in this study

Strain	Relevant genotype	Donor	Recipient	Target gene	Reference
PFM2	MG1655 *rph*$^{+}$				(1)
PFM5	Δ*mutL*				(1)
WX320	Δ*oriC oriZ*$^{+}$ (AB1157)				(12)
WX340	*oriC*$^{+}$ *oriZ*$^{+}$ (AB1157)				(12)
PF11	AB1157				Lab strain
PFM118	Δ*umuDC* Δ*dinB* Δ*mutL*				(10)
PFM120	*lexA3* Δ*sulA* Δ*mutL*				This Study
PFM163	*mutD5*				(13)
PFM165/397/399	*mutD5* Δ*mutL*				(13)
PFM244	Δ*mutL, scarless*				(10)
PFM256	Δ*tus* Δ*mutL*	JW1602	PFM244	Δ*tus::*Kn^{R}	This Study
PFM257	Δ*matP* Δ*mutL*	JW0939	PFM244	Δ*matP::*Kn^{R}	This Study
PFM258	Δ*hupA* Δ*mutL*	JW3964	PFM244	Δ*hupA::*Kn^{R}	This Study
PFM259	Δ*hupB* Δ*mutL*	JW0430	PFM244	Δ*hupB*::Kn^{R}	This Study
PFM317/ 318	Δ*fis* Δ*mutL*	JW3229	PFM244	Δ*fis::*Kn^{R}	This Study
PFM342/343	Δ*mutS, scarless*				(10)
PFM421	Δ*rnhA* Δ*mutL*	JW0204	PFM244	Δ*rnhA*::Kn^{R}	This Study
PFM422	Δ*recA* Δ*mutL*	JW2669	PFM244	Δ*recA::*Kn^{R}	This Study

PFM424	Δ*recA* Δ*mutS*	JW2669	PFM342	Δ*recA::Kn*^{R}	This Study
PFM426	Δ*oriC oriZ*$^+$ Δ*mutL* (AB1157)	JW4128	WX320	Δ*mutL::*Kn^R	This Study
PFM430/ 431	*oriC*$^+$ *oriZ*$^+$ Δ*mutL* (AB1157)	JW4128	WX340	*ΔmutL::*Kn^R	This Study
PFM456	Δ*recB* Δ*mutL*	JW2788	PFM244	Δ*recB::*Kn^R	This Study
PFM482	Δ*fis* Δ*mutS*	JW3229	PFM343	Δ*fis::*Kn^R	This Study
PFM533/ 534	Δ*seqA* Δ*mutL*	JW0674	PFM244	Δ*seqA::*Kn^R	This Study
PFM661	Δ*hupA* ΔrecA Δ*mutL*	JW2669	PFM258	Δ*recA::Kn*^{R}	This Study
PFM669	Δ*mutL* (AB1157)	JW4128	PF11	Δ*mutL::*Kn^R	This Study
PFM677	Δ*rep* Δ*mutL*	JW5604	PFM244	Δ*rep::*Kn^R	This Study
PFM713	Δ*dps* Δ*mutL*	JW0797	PFM244	Δ*dps::*Kn^R	This Study
PFM741	Δ*hns* Δ*mutL*	JW1225-2	PFM244	Δ*hns::*Kn^R	This Study
PFM799	Δ*nrdR ΔmutL*	JW0403	PFM244	Δ*nrdR:*:Kn^R	This Study
DK2140/2141/ 2142/2143	*Bacillus subtilis mutS::*Tn*10*				M. Konkol & D. Kearns, personal communication

In all strains the Kn^R element was removed by FLP recombination (5).

Scarless: Scarless gene deletion using a cat-I-SceI cassette (14).

Table S2. Oligonucleotides used in this study

Relevant gene	Name	Sequence	Reference
mutL	mutL Fw	5′-GCCTGCGCAATTACTTCCTTG-3′	(1)
	mutL Rv	5′-CGCAGCTCAATGGCTAACGC-3′	
mutS	mutS FW	5'-CACGAGAGATACGCTTGCC-3'	This study
	mutS RV	5'-TCGTGGTTGCCTTTAACCGA-3'	
oriC	mioC_2958 FW	5'-CAAATAAGTATACAGATCGTG-3'	This study
	oriC dwnstrmRV	5'-CTTTGTCGGCTTGAGAAAGAC-3'	
oriZ	yahL1146FW	5'-GAGATGATGCGCGATTAAATG-3'	This study
	yahMupstrmRV	5'-CCCCGTACCATACAACAATC-3'	
rnhA	rnhA_dwnstrm RV	5'-CATCGGATTTAGCGTTAAAG-3'	This study
	rnhA_dwnstrm FW	5'-CTTTAACGCTAAATCCGATG-3'	
seqA	seqAFW	5'-CGAGTTTGTGCGTCCGATTC-3'	This study
	seqARV	5'-GATGGCATTGGAAACGGCAG-3'	
tus	tus FW	5'-CTCGTGCAAGGCCATTATGC-3'	This study
	tus RV	5'-AGTTTGACAGCTGGGTACGG-3'	
matP	matP FW	5'-ACAATACTCCTGGCATGGGC-3'	This study
	matP RV	5'-TGACGCTTACAACCAGGGTC-3'	
recA	recAF0102	5'-GCATTGCAGACCTTGTGGC-3'	This study
	recAR1134	5'-CGACGGGATGTTGATTCTG-3'	
rnhA	rnhA_dwnstrm RV	5'-CATCGGATTTAGCGTTAAAG-3'	This study
	rnhA_dwnstrm FW	5'-CTTTAACGCTAAATCCGATG-3'	

recD	recD_RV	5'-GACCACGCGCAGTATTCACT-3'	This study
	recD_FW	5'-GGGTGAAGACAGTTCGGCTT-3'	
recB	recB_RV	5'-GTTCATCTCCCCTGCTGACC-3'	This study
	recB_FW	5'-CGTTTTTCCCAACCGCAGAG-3'	
fis	fisRV	5'-CTTTTTCAGAACGCGGTGGC-3'	This study
	fisFW	5'-GGAACACGCTCCAAATGACC-3'	
hupA	hupAFW	5'-CAGGCTGGTCGCGAAATGAG-3'	This study
	hupARV	5'-GCTAAACACGGCAAGCAGATG-3'	
hupB	hupBFW	5'-CTGTGAAGCGCATTGAGGAAG-3'	This study
	hupBRV	5'-CTTGAGCACGAGACTGTTTGC-3'	
dps	dpsFW_G	5'-GGGGTCTACGCTGACAGTAC-3'	This study
	dpsRV_BAN	5'-GATGCACCATTCTGGGGCACC-3'	
hns	hnsRV_G	5'-GTGGTAGAAAAACCGAAAGC-3'	This study
	hnsFW_G	5'-CATGAATCAGGAAGTTTTAAC-3'	
rep	repRv	5'-CTGTTGACCTTGACGCTTCC-3'	This study
	repFw	5'-CTTTGGCCCAACGAATCTGC-3'	

Table S3. Experimental data

Strain	Description	No. of BPSs	No. of MA lines	Total no. of generations	BPSs per generation x 10^3	95% CL
*Collective	MMR$^-$	30061	334	264958	113	2
PFM421	Δ*rnhA* Δ*mutL*	3198	39	22690	141	7
PFM669	Δ*mutL* (AB1157)	1334	33	18850	71	6
PFM430/ 431	*oriC*$^+$ *oriZ*$^+$ Δ*mutL* (AB1157)	3150	65	33607	94	6
PFM426	Δ*oriC oriZ*$^+$ Δ*mutL (AB1157)*	3544	45	25176	141	9
PFM533/ 534	Δ*seqA* Δ*mutL*	1855	44	20927	89	7
*PFM5m	Δ*mutL* on minimal medium	1435	48	28197	51	3
*PFM343m	Δ*mutS* on minimal medium	1608	46	26280	61	4
*PFM343VBs	Δ*mutS* on supplemented minimal medium	2476	39	23017	108	5
*PFM343dLB	Δ*mutS* on diluted LB	3546	40	22495	158	8
*PFM342LTM	Δ*mutS* at low temperature	1259	44	24875	51	5
PFM799	Δ*nrdR* Δ*mutL*	5272	42	23581	224	12
PFM677	Δ*rep* Δ*mutL*	3258	43	23961	136	7
PFM256	Δ*tus* Δ*mutL*	3672	28	32967	111	10
PFM257	Δ*matP* Δ*mutL*	3979	33	36725	108	7

PFM422	Δ*recA* Δ*mutL*	6797	40	39713	171	11
PFM424	Δ*recA* Δ*mutS*	6266	36	36340	172	11
PFM456	Δ*recB* Δ*mutL*	3321	46	20598	161	9
*PFM118	Δ*umuDC* Δ*dinB* Δ*mutL*	1110	23	12078	92	41
PFM120	*lexA3* Δ*sulA* Δ*mutL*	2909	33	19853	147	13
PFM259	Δ*hupB* Δ*mutL*	3910	32	36390	107	8
PFM258	Δ*hupA* Δ*mutL*	2075	26	27315	76	7
PFM317/ 318	Δ*fis* Δ*mutL*	7616	35	37731	202	14
PFM482	Δ*fis* Δ*mutS*	4669	40	22687	206	12
PFM741	Δ*hns* Δ*mutL*	3367	46	25551	132	5
PFM713	Δ*dps* Δ*mutL*	2927	40	23377	125	8
†PFM163	*mutD5*	13625	26	3481	3915	344
†PFM165/397/399	*mutD5* Δ*mutL*	40686	75	7012	5802	456
*Collective	Wild Type	1933	341	2015066	0.96	0.10
‡Collective	*Bacillus subtilis mutS::*Tn*10*	10551	71	171805	61	3

*Data are from (10)

†Data are from (13)

‡Data are combined from four MA experiments with DK2140 (NCIB3610 *mutS*::Tn*10*), DK2141 (NCIB3610 *mutS*::Tn*10*), DK2142 (NCIB3610 *mutS*::*Tn10* Δ*comI*), and DK2143 (NCIB3610 *mutS*::Tn*10* Δ*comI*). There were no differences in mutation rates or spectra among these strains

Supplemental References

1. Lee H, Popodi E, Tang H, Foster PL. Rate and molecular spectrum of spontaneous mutations in the bacterium *Escherichia coli* as determined by whole-genome sequencing. Proceedings of the National Academy of Sciences of the United States of America. 2012;109(41):E2774-E83.
2. Dewitt SK, Adelberg EA. The Occurrence of a Genetic Transposition in a Strain of Escherichia Coli. Genetics. 1962;47(5):577-85.
3. Baba T, Ara T, Hasegawa M, Takai Y, Okumura Y, Baba M, et al. Construction of *Escherichia coli* K-12 in-frame, single-gene knockout mutants: the Keio collection. Mol Syst Biol. 2006;2:2006.
4. Miller JH. Experiments in molecular genetics. Cold Spring Harbor, N.Y.: Cold Spring Harbor Laboratory; 1972 1972.
5. Datsenko KA, Wanner BL. One-step inactivation of chromosomal genes in *Escherichia coli* K-12 using PCR products. Proc Natl Acad Sci USA. 2000;97:6640-5.
6. Miller JH. A short course in bacterial genetics: a laboratory manual and handbook for *Escherichia coli* and related bacteria. Cold Spring Harbor: Cold Spring Harbor Laboratory Press; 1992 1992.
7. Foster PL. Methods for determining spontaneous mutation rates. Methods Enzymol. 2006;409:195-213.
8. Hall BM, Ma CX, Liang P, Singh KK. Fluctuation analysis CalculatOR: a web tool for the determination of mutation rate using Luria-Delbruck fluctuation analysis. Bioinformatics. 2009;25(12):1564-5.

97 9. Foster PL, Lee H, Popodi E, Townes JP, Tang H. Determinants of spontaneous mutation in
98 the bacterium *Escherichia coli* as revealed by whole-genome sequencing. Proceedings of the
99 National Academy of Sciences of the United States of America. 2015;112(44):E5990-E599.
100 10. Foster PL, Niccum BA, Popodi E, Townes JP, Lee H, MohammedIsmail W, et al.
101 Determinants of base-pair substitution patterns revealed by whole-genome sequencing of DNA
102 mismatch repair defective *Escherichia coli*. Genetics. 2018;209(4):1029-42.
103 11. Li H, Durbin R. Fast and accurate short read alignment with Burrows-Wheeler transform.
104 Bioinformatics. 2009;25(14):1754-60.
105 12. Wang X, Lesterlin C, Reyes-Lamothe R, Ball G, Sherratt DJ. Replication and segregation of
106 an Escherichia coli chromosome with two replication origins. Proceedings of the National
107 Academy of Sciences of the United States of America. 2011;108(26):E243-50.
108 13. Niccum BA, Lee H, MohammedIsmail W, Tang H, Foster PL. The spectrum of replication
109 errors in the absence of error correction assayed across the whole genome of *Escherichia coli*.
110 Genetics. 2018;209(4):1043-54.
111 14. Blank K, Hensel M, Gerlach RG. Rapid and highly efficient method for scarless
112 mutagenesis within the *Salmonella enterica* chromosome. PLoS One. 2011;6(1):e15763.
113
114

115 ## Supplementary Figure Legends

116 **Supplementary Figure S1**. The BPS density pattern is not due to transcription but is affected by
117 moving the origin of replication. Shown are plots of the wavelet coherence between two
118 binned BPS data sets. The colors give the magnitude-squared coherence, a measure of the
119 correlation between the data sets, according to the scale on the left. The dotted line gives the
120 "cone of influence" within which the results are free of artifactual edge effects. Arrows indicate
121 the phase-lag between the two data sets; arrows pointing right indicate in-phase, arrows
122 pointing left indicate 180° out-of-phase, and arrows pointing in other directions indicate the
123 various degrees in between. **Supplementary Figure S1A**. The wavelet coherence between the
124 binned BPS data from the MMR-defective strains taken in the clockwise and counterclockwise
125 directions around the chromosome. This presentation illustrates the almost complete
126 symmetry of the BPS density pattern. **Supplementary Figure S1B.** Plot of the wavelet coherence
127 between the BPS data from the MMR-defective strains and the mean binned reads from RNA-
128 Seq samples taken during lag, log, and stationary growth phases of the Δ*mutL* mutant strain,
129 PFM144. **Supplementary Figures S1C, D, E, and F**. Plots of the wavelet coherence between the
130 binned BPS data from the MMR-defective strains and the indicated mutant strains. See text for
131 a description of the strains. Strains: S1C, PFM421; S1D, PFM430/431; S1E, PFM426; S1F,
132 PFM533/534.

133 **Supplementary Figure S2**. Altering the progression of DNA replication affects the BPS density
134 pattern. Plots of the wavelet coherence between the binned BPS data from the MMR-defective
135 strains and the indicated mutant strains. The colors give the magnitude-squared coherence, a
136 measure of the correlation between the data sets, according to the scale on the left. The dotted

137 line gives the "cone of influence" within which the results are free of artifactual edge effects.
138 Arrows indicate the phase-lag between the two data sets; arrows pointing right indicate in-
139 phase, arrows pointing left indicate 180° out-of-phase, and arrows pointing in other directions
140 indicate the various degrees in between. **Supplementary Figures S2A, B, C, and D**. Altering the
141 cellular growth rate by growing a Δ*mutS* mutant strain on different medium and at different
142 temperatures differentially affects the BPS density pattern. In the experiments shown in Plot A,
143 C, and D, the cells grew at about half the normal rate, whereas in the experiment shown in plot
144 B they grew at the normal rate. Strains: S2A, B, and C, PFM343; S2D, PFM342. **Supplementary**
145 **Figures S2E and F.** Dysregulation of dNTP levels and loss of Rep, the auxiliary replication
146 helicase, affect the BPS density pattern. Strains: S2E, PFM799; S2F, PFM677. **Supplementary**
147 **Figures S2G and H**. Loss of the Tus antihelicase has no effect, but loss of the terminus
148 organizing protein, MatP, changes the BPS density pattern across the chromosome. Strains:
149 S2G, PFM256; S2H, PFM257.
150 **Supplementary Figure S3**. Loss of RecA, HUα, or Fis changes the BPS pattern, but the SOS
151 response and other NAPs do not. For a description of the plots, see the legend to
152 Supplementary Figure S2. **Supplementary Figures S3A, B, and C.** Loss of RecA alters the BPS
153 density pattern in the terminus region, but not through its role as a master regulator of the SOS
154 response. RecA (Figure S3A) is *E. coli*'s major recombinase. The *umuDC* and *dinB* genes (Figure
155 S3B) encode error-prone DNA polymerases that are induced as part of the SOS response. The
156 *lexA3* allele encodes a non-inducible repressor of the SOS genes. Deletion of *sulA* prevents
157 lethal filamentation, which is not relevant to this study. Strains: S3A, PFM422; S3B, PFM118;
158 S3C, PFM120. **Supplementary Figures S3D, E, F, G, and H**. Loss of the HUα subunit of HU or of

159 Fis changes the BPS density pattern, but loss of the HUβ subunit of HU, HNS, or DPS have only
160 minor effects. Strains: S3D, PFM259; S3E, PFM258; S3F, PFM317/318; S3G, PFM741/742; S3H,
161 PFM713.
162 **Supplementary Figure S4**. The BPS density pattern is a result of biased correction by replication
163 proofreading and MMR. For a description of the plots, see the legend to Supplementary Figure
164 S2. **Supplementary Figures S4A and B**. A strain with deficient proofreading but active MMR
165 yields a BPS pattern similar to a MMR-defective strain, but a strain with neither proofreading
166 nor MMR does not. The *mutD5* allele encodes an exonuclease-deficient proofreader. Strains:
167 S4A, PFM163; S4B, PFM165/397/399. **Supplementary Figures S4C and D**. The BPS density
168 pattern in the wild-type strain does not match the pattern of either the MMR-defective strain,
169 or the mutD5 mutant strain. Strains: S4C and D, eight strains with wild-type mutational
170 phenotypes (see text). **Supplementary Figures S4E and F**. MMR-defective *B. subtilis* also has a
171 symmetrical BPS density pattern, but it is different than *E. coli*'s pattern. Strains: three *B.*
172 *subtilis* mutant strains with the same mutational phenotype (see Supplemental Tables S1 and
173 S3).
174 **Supplementary Figure S5**: The BPS density patterns from experiments mentioned in the text
175 but not shown. For each plot the data were collected into 100 Kb bins starting at the origin of
176 replication on the left and continuing around the chromosome back to the origin. The BPS
177 density patterns (bars) and Daubechies wavelet transforms (pink lines) of the indicated strains
178 are compared to the Daubechies wavelet transform of the combined MMR$^-$ strains (grey line).
179 In each plot the left-hand scale has been adjusted to bring the wavelets close together for

180 comparison. Strains: S5A, MMR strains but A:T transitions at 5'NAC3'/3'NTG5' sites removed;

181 S5B, PFM669; S5C, PFM5; S5D, PFM424; S5E, PFM456; S5F, PFM482.

182 **Supplementary Figure S6**: Plots of the wavelet coherence between the binned BPS data from

183 the MMR-defective strains and the data from the experiments shown in Supplementary Figure

184 S5. See the legends from Supplementary Figure S2 and S5 for details

Supplementary Figure S1

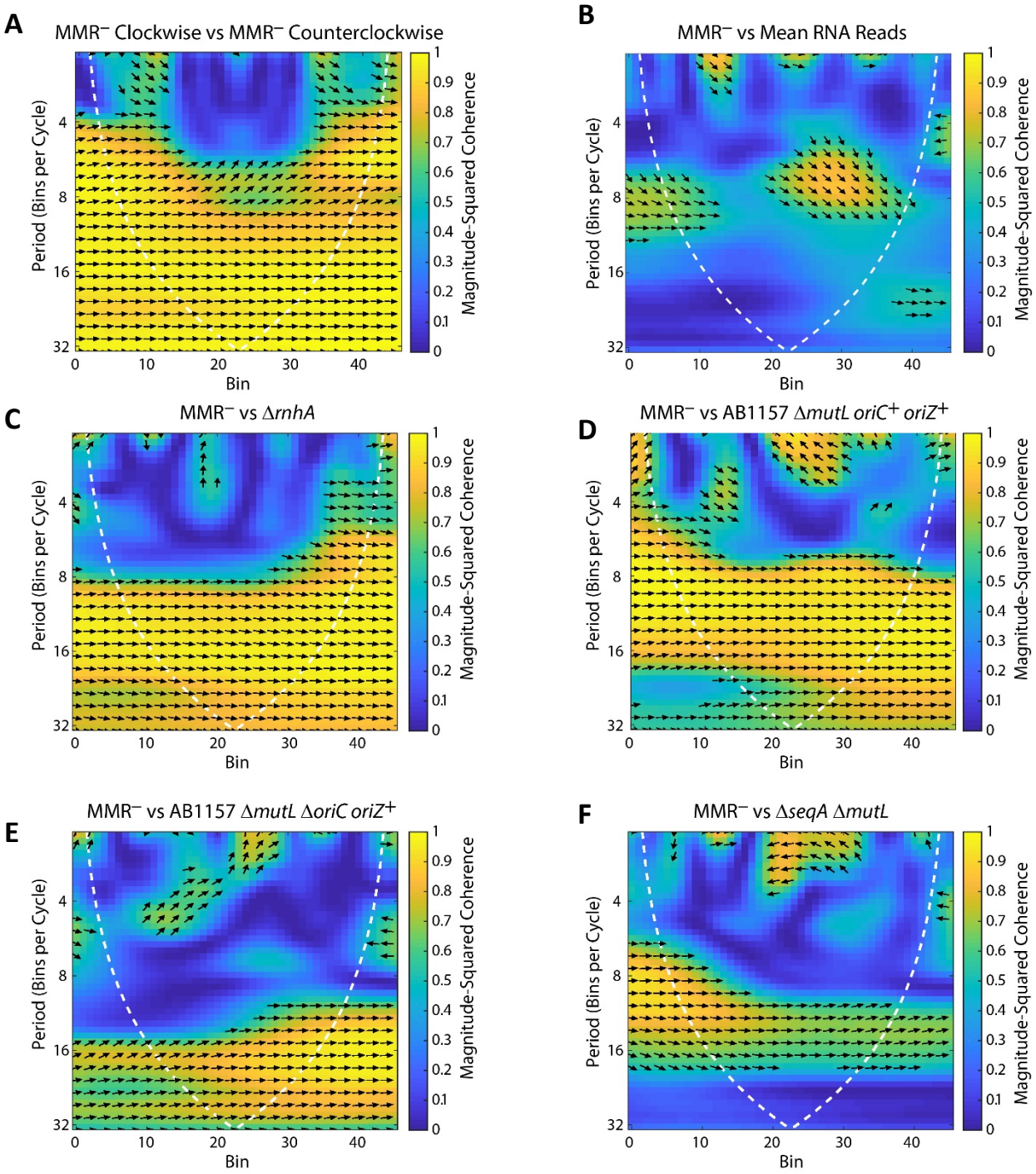

Supplementary Figure S2

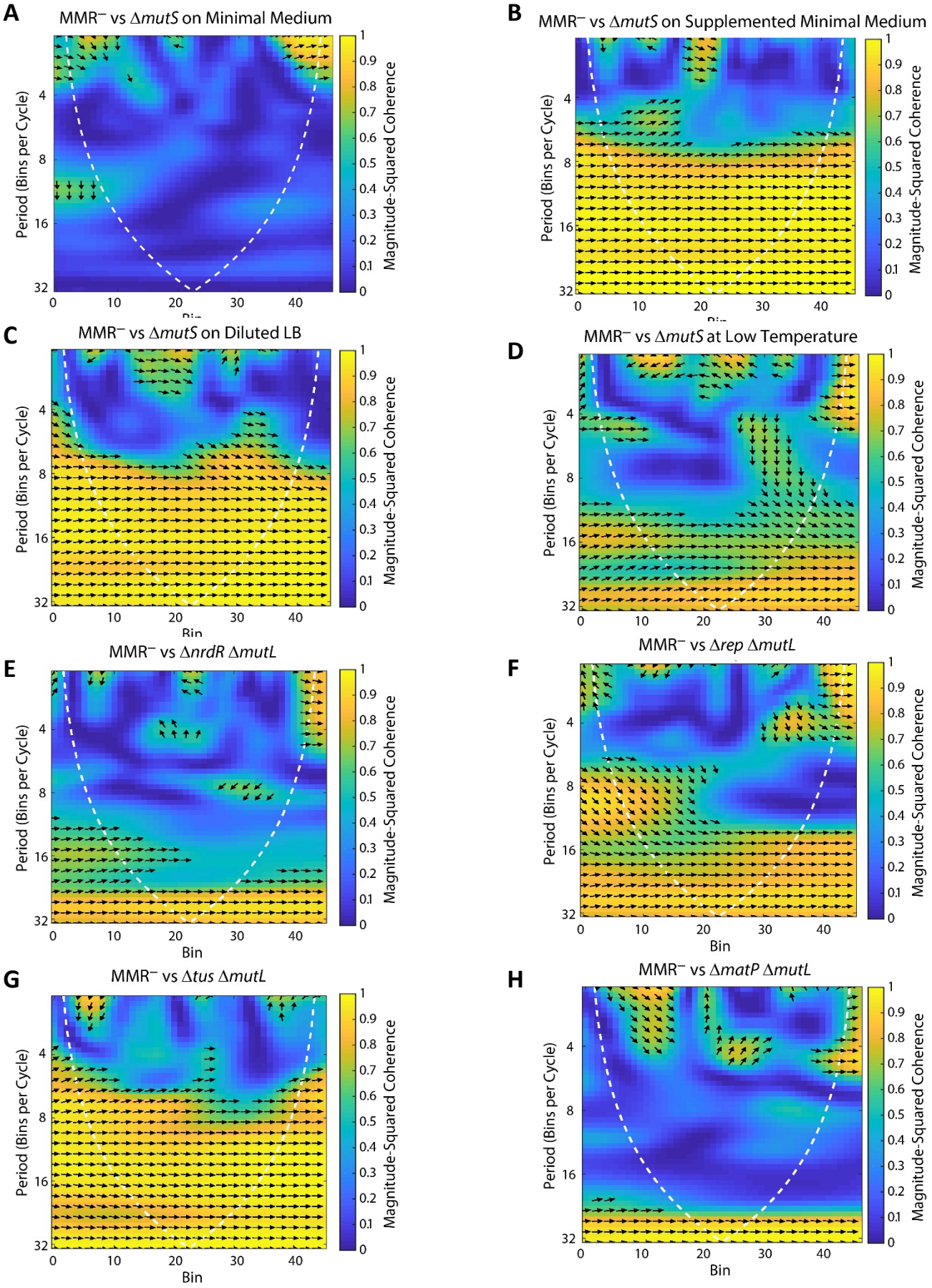

Supplementary Figure S3

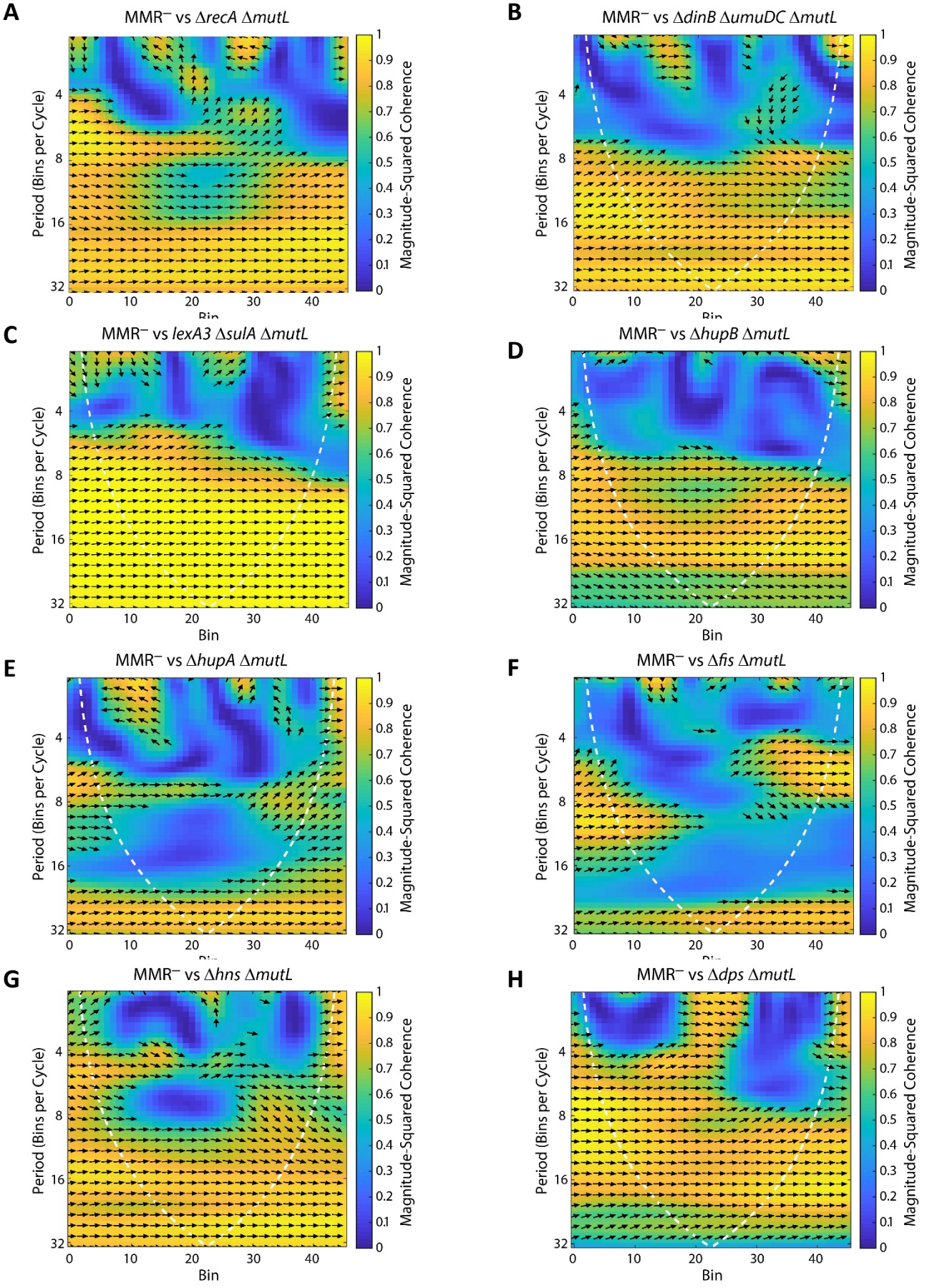

Supplementary Figure S4

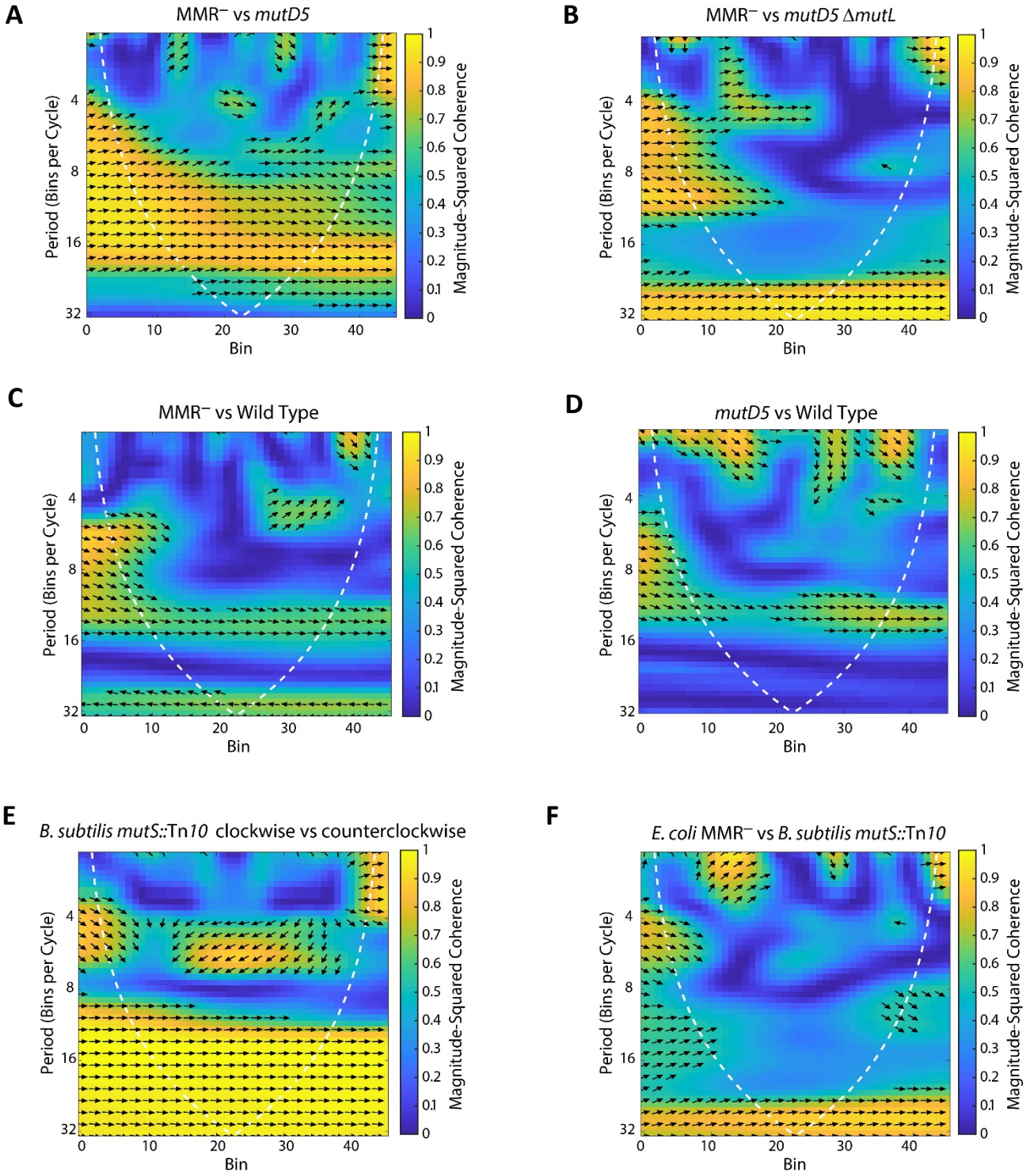

Supplementary Figure S5

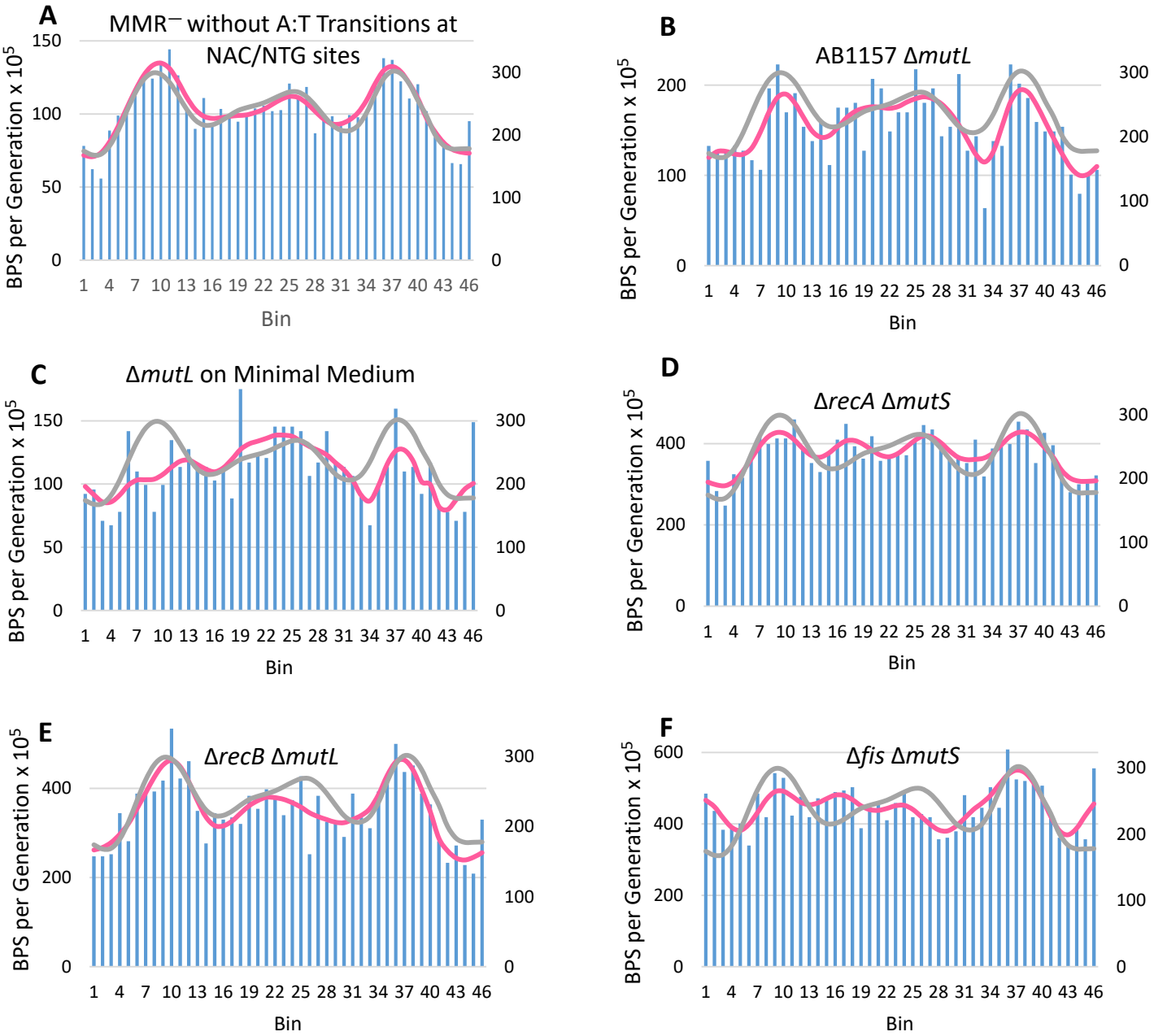
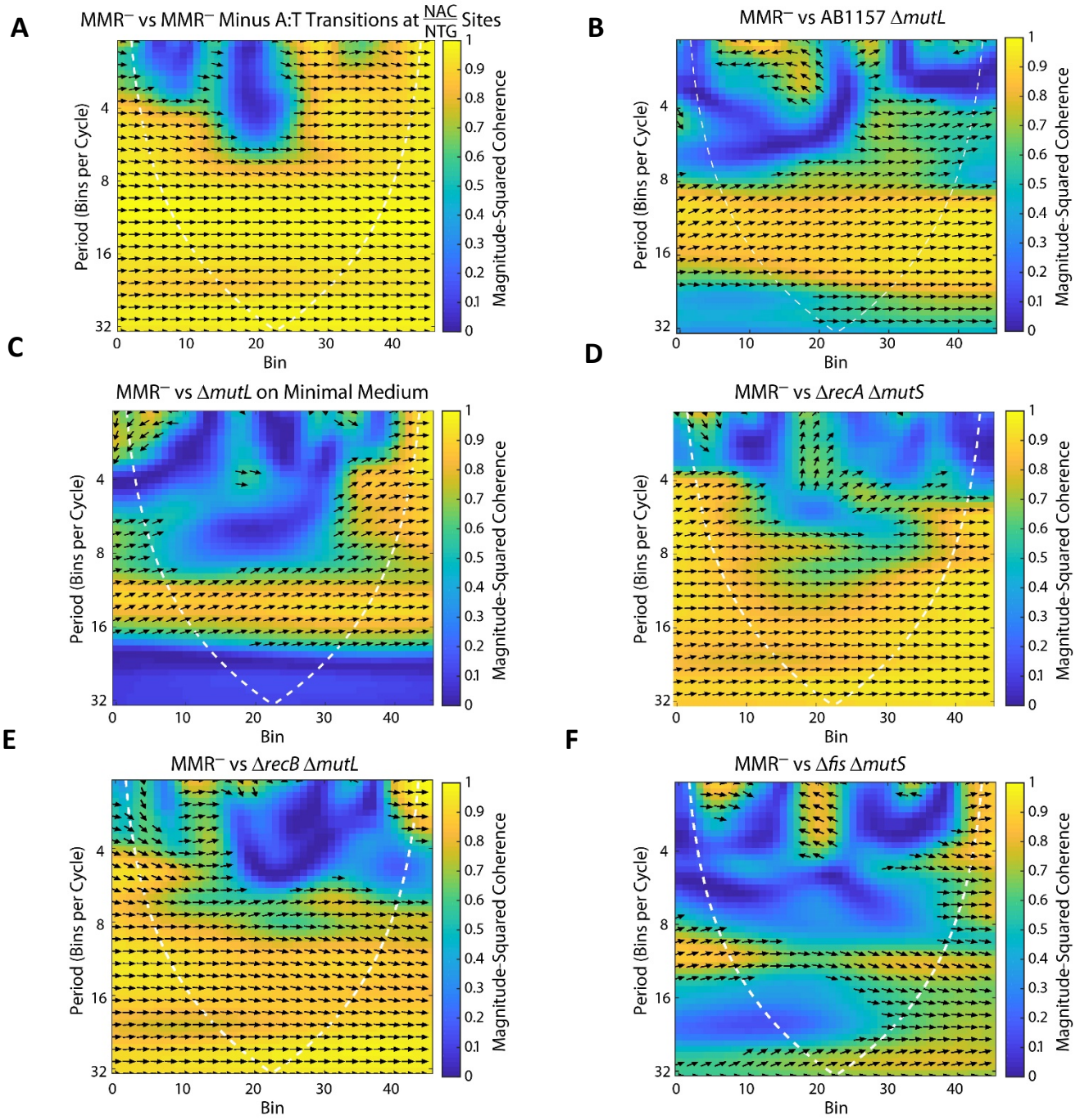
Supplementary Figure S6